



HAL
open science

PDX1.1-dependent biosynthesis of vitamin B6 protects roots from ammonium-induced oxidative stress

Ying Liu, Rodolfo A Maniero, Ricardo F.H. Giehl, Michael Melzer, Priscille Steensma, Gabriel Krouk, Teresa B Fitzpatrick, Nicolaus von Wirén

► To cite this version:

Ying Liu, Rodolfo A Maniero, Ricardo F.H. Giehl, Michael Melzer, Priscille Steensma, et al.. PDX1.1-dependent biosynthesis of vitamin B6 protects roots from ammonium-induced oxidative stress. *Molecular Plant*, 2022, 15 (5), pp.820-839. 10.1016/j.molp.2022.01.012 . hal-03540746

HAL Id: hal-03540746

<https://hal.inrae.fr/hal-03540746>

Submitted on 24 Jan 2022

HAL is a multi-disciplinary open access archive for the deposit and dissemination of scientific research documents, whether they are published or not. The documents may come from teaching and research institutions in France or abroad, or from public or private research centers.

L'archive ouverte pluridisciplinaire **HAL**, est destinée au dépôt et à la diffusion de documents scientifiques de niveau recherche, publiés ou non, émanant des établissements d'enseignement et de recherche français ou étrangers, des laboratoires publics ou privés.

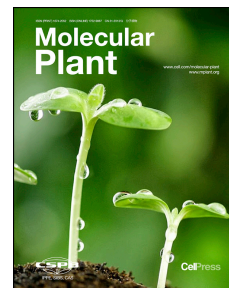


Distributed under a Creative Commons Attribution 4.0 International License

Journal Pre-proof

PDX1.1-dependent biosynthesis of vitamin B₆ protects roots from ammonium-induced oxidative stress

Ying Liu, Rodolfo A. Maniero, Ricardo F.H. Giehl, Michael Melzer, Priscille Steensma, Gabriel Krouk, Teresa B. Fitzpatrick, Nicolaus von Wirén



PII: S1674-2052(22)00012-0
DOI: <https://doi.org/10.1016/j.molp.2022.01.012>
Reference: MOLP 1310

To appear in: *MOLECULAR PLANT*
Accepted Date: 17 January 2022

Please cite this article as: **Liu Y., Maniero R.A., Giehl R.F.H., Melzer M., Steensma P., Krouk G., Fitzpatrick T.B., and von Wirén N.** (2022). PDX1.1-dependent biosynthesis of vitamin B₆ protects roots from ammonium-induced oxidative stress. *Mol. Plant*. doi: <https://doi.org/10.1016/j.molp.2022.01.012>.

This is a PDF file of an article that has undergone enhancements after acceptance, such as the addition of a cover page and metadata, and formatting for readability, but it is not yet the definitive version of record. This version will undergo additional copyediting, typesetting and review before it is published in its final form, but we are providing this version to give early visibility of the article. Please note that, during the production process, errors may be discovered which could affect the content, and all legal disclaimers that apply to the journal pertain.

© 2022 The Author

1 **PDX1.1-dependent biosynthesis of vitamin B₆ protects roots from ammonium-**
2 **induced oxidative stress**

3 Ying Liu¹, Rodolfo A. Maniero¹, Ricardo F.H. Giehl¹, Michael Melzer², Priscille
4 Steensma³, Gabriel Krouk⁴, Teresa B. Fitzpatrick³, Nicolaus von Wirén^{1,*}

5
6 ¹ Molecular Plant Nutrition, ²Structural Cell Biology, Leibniz Institute of Plant Genetics
7 and Crop Plant Research (IPK), Corrensstrasse 3, 06466 Gatersleben, Germany

8 ³ Department of Botany and Plant Biology, University of Geneva, 1211 Geneva,
9 Switzerland

10 ⁴ BPMP, Univ Montpellier, CNRS, INRA, SupAgro, Montpellier, France

11 * Corresponding Author: vonwiren@ipk-gatersleben.de

12
13 ORCID IDs: 0000-0001-5753-4247 (Y.L.); 0000-0002-1074-8034 (R.A.M.); 0000-
14 0003-1006-3163 (R.F.H.G.); 0000-0002-5213-4030 (M.M.); 0000-0002-3628-2228
15 (P.S.); 0000-0003-3693-6735 (G.K.); 0000-0001-7694-5631 (T.B.F.); 0000-0002-
16 4966-425X (N.v.W.)

17

18 **Running title:** Vitamin B₆ alleviates ammonium toxicity

19

20 **Keywords:** ammonium nutrition, apoplastic pH, Fe mobilization, root elongation,
21 pyridoxine, ROS scavenging.

22

23 **SHORT SUMMARY:** Ammonium supply triggers a localized Fe-dependent oxidative
24 burst that arrests primary root elongation but also induces PDX1.1-dependent vitamin
25 B₆ production to quench ammonium-induced ROS formation.

26

27 **ABSTRACT**

28 Despite serving as a major inorganic nitrogen source for plants, ammonium causes
29 toxicity at elevated concentrations, inhibiting root elongation early on. While previous
30 studies have shown that ammonium-inhibited root development relates to ammonium
31 uptake and formation of reactive oxygen species (ROS) in roots, it remained open
32 which mechanisms are underlying the repression of root growth and how plants cope
33 with this inhibitory effect of ammonium. Here, we demonstrate that ammonium-
34 induced apoplastic acidification co-localizes with Fe precipitation and hydrogen

35 peroxide (H_2O_2) accumulation along the stele of the elongation and differentiation
36 zone in root tips, indicating Fe-dependent ROS formation. By screening ammonium
37 sensitivity in T-DNA insertion lines of ammonium-responsive genes, we identified
38 *PDX1.1*, which is upregulated by ammonium in the root stele and catalyzes
39 biosynthesis *de novo* of vitamin B₆. Root growth of *pdx1.1* mutants is hypersensitive
40 to ammonium, while chemical complementation or overexpression of *PDX1.1*
41 restores root elongation. This salvage strategy requires non-phosphorylated forms of
42 vitamin B₆ that are able to quench reactive molecular oxygen species and rescue root
43 growth from ammonium inhibition. We propose *PDX1.1*-mediated synthesis of non-
44 phosphorylated B₆ vitamers as a primary strategy to protect roots from ammonium-
45 dependent ROS formation.

46

47

48 INTRODUCTION

49 Nitrogen (N) is an essential mineral element for plant development and extensively
50 applied in crop production (Xu et al., 2012). While synthetic N fertilizers greatly
51 improve global crop yield, the input of nitrate-based N fertilizers also bears
52 environmental risks when leached as nitrate or emitted as nitrogen oxide (Ju et al.,
53 2009; Sutton et al., 2011). Since ammonium is less prone to leaching than nitrate,
54 ammonium-based N fertilizers are widely used nowadays to replace nitrate in
55 agricultural plant production. To increase fertilizer use efficiency, ammonium is often
56 supplied in locally restricted fertilizer strips, where it is present at very high
57 concentrations (Nkebiwe et al., 2016). Although ammonium is a preferential inorganic
58 N source for many plant species (Gazzarrini et al., 1999), excessive ammonium
59 causes toxicity resulting in leaf chlorosis and suppressed root growth (Britto and
60 Kronzucker, 2002). These symptoms rely on ammonium triggering multiple
61 physiological and morphological responses, including changes in apoplastic and
62 cytosolic pH, gene expression, protein modification, ion transport, N metabolism,
63 redox and phytohormone status, as well as root system architecture (Britto and
64 Kronzucker, 2002; Li et al., 2014; Liu and von Wirén, 2017). Against this background
65 and with the increasing use of ammonium-based N fertilizers in agricultural nutrient
66 management, it is important to obtain a deeper understanding of how roots adapt to
67 an ammonium-replete environment.

68 The most typical morphological changes in root system architecture of ammonium-
69 exposed roots are arrested elongation of primary and lateral roots and enhanced
70 branching of lateral roots (Li et al., 2010; Lima et al., 2010; Liu et al., 2013).
71 Regarding lateral root branching, it has recently been shown that apoplastic
72 acidification caused by AMMONIUM TRANSPORTER (AMT)-mediated ammonium
73 uptake provokes pH-dependent radial auxin diffusion to stimulate locally the
74 emergence of lateral root primordia, forming a highly branched root system (Meier et
75 al., 2020). Given that in several auxin-related mutants root elongation is still as
76 sensitive to ammonium as in wild-type plants, the repression of root elongation by
77 ammonium is unlikely due to altered distribution or action of auxin in plants (Li et al.,
78 2010; Liu et al., 2013). Thus, altered root elongation and lateral root branching under
79 ammonium supply are most likely governed by distinct mechanisms. Neither root
80 elongation nor lateral root branching can be triggered by glutamine, the primary
81 assimilation product of ammonium (Lima et al., 2010; Rogato et al., 2010),

82 suggesting that ammonium itself or ammonium-related metabolites or signals are
83 critical for root development (Liu and von Wirén, 2017). Indeed, excessive
84 ammonium accumulation and hypersensitive root growth of the *cipk23* mutant
85 indicated that ammonium-induced calcium signaling is required to re-adjust internal
86 NH_4^+/K^+ ratios (Shi et al., 2020). This refers to the function of CIPK23, a CBL-
87 interacting protein kinase, in modulating AMT-, HAK- and AKT-type transporter
88 activities (Ragel et al., 2015; Straub et al., 2017; Sanchez-Barrena et al., 2020; Dong
89 et al., 2021) with strong impact on cytosolic ammonium accumulation and root growth.
90 A further ammonium-related signal may be ethylene, which appears to modulate
91 genes involved in ammonium uptake and assimilation via the transceptor function of
92 NRT1.1 (Jian et al., 2018). Even though these signaling processes help maintaining
93 cytosolic ammonium homeostasis, they do not explain ammonium-dependent root
94 growth inhibition.

95 Horizontal split agar experiments indicate that the critical region to sense the
96 inhibitory effect of ammonium on root elongation is the root tip (Li et al., 2010). At the
97 cellular level, both cell division and cell elongation are substantially repressed by
98 ammonium, while the integrity of the root stem cell niche remains unaffected (Liu et
99 al., 2013). On the search for mutants overcoming ammonium-induced root growth
100 inhibition, the *vtc1-1* mutant was isolated, which is defective in GMP-mannose
101 pyrophosphorylase (GMPase) and thus not only in downstream ascorbate
102 biosynthesis but also in N-glycosylation of proteins (Qin et al., 2008). However,
103 despite its significant impact on ammonium fluxes (Li et al., 2010), GMPase activity
104 turned out not to be the primary cause of ammonium-dependent root growth inhibition
105 (Kempinski et al., 2011). Transcriptome studies have indicated that enhanced
106 formation of ROS is a typical ammonium-related physiological response (Patterson et
107 al., 2010). Even though significantly higher steady-state H_2O_2 levels in roots were not
108 detected, antioxidative defense systems were induced that comprise ROS-degrading
109 enzymes, including superoxide dismutase, catalase, peroxidase, guaiacol peroxidase
110 and glutathione reductase (Patterson et al., 2010). However, in leaves ammonium
111 toxicity increased H_2O_2 formation, which was found to be mediated by ethylene and
112 followed by enhanced peroxidase activity probably via ABA signaling (Li et al., 2019;
113 Sun et al., 2020). Also in the roots of rice, ammonium treatment increased H_2O_2
114 contents and induced the heme-heme oxygenase *OsSE5* together with other ROS-
115 detoxifying enzymes including superoxide dismutase, catalase, and ascorbate

116 peroxidase to relieve ammonium-supplied plants from oxidative stress (Xie et al.,
117 2015). These studies indicate that ammonium toxicity causes ROS formation and that
118 the capacity of enzymatic ROS detoxification is a major determinant of ammonium
119 tolerance in plants. So far, evidence for the involvement of non-enzymatic
120 antioxidants in ammonium-induced oxidative stress defense was not obtained,
121 considering that in roots the pool sizes and oxidative states of NADH, NADPH,
122 glutathione and ascorbate were not substantially altered by ammonium supply
123 (Patterson et al., 2010).

124 To explore the mechanisms by which ammonium-exposed roots cope with
125 ammonium toxicity and ammonium-dependent ROS formation, we first used a
126 pharmacological approach unraveling localization of the ammonium-triggered H₂O₂
127 burst. We then screened mutants of ammonium-responsive genes in roots and
128 identified *PDX1.1*, a gene involved in the biosynthesis *de novo* of vitamin B₆.
129 Chemical complementation and genetic approaches showed that non-
130 phosphorylated forms of vitamin B₆ suppressed H₂O₂ formation under ammonium
131 supply. With *PDX1.1*-dependent vitamin B₆ formation, our study identifies a protective
132 mechanism that spatially overlaps with ammonium-triggered H₂O₂ formation in inner
133 root cells and thus carries potential to better adapt plant roots to ammonium-based
134 fertilization strategies.

135

136 RESULTS

137 Accumulation of H₂O₂ under ammonium supply inhibits primary root 138 elongation

139 When wild-type seedlings of *Arabidopsis* were grown on half-strength MS medium for
140 6 d in the presence of either 1 or 10 mM ammonium as the sole N source, primary
141 root length became 25 or 35% shorter, respectively, than that of nitrate-grown plants
142 (Fig S1A, B). Likewise, total and mean length of lateral roots were repressed to a
143 similar extent as primary root length, suggesting a common mechanism underlying
144 ammonium-induced growth inhibition in both root types (Fig S1B-D). A significant
145 dose-dependent decrease in root elongation rate set in already after 1 d of
146 ammonium exposure suggesting a rapid inhibitory mechanism (Fig S1E-G). Root
147 exposure to ammonium decreased both, cortical cell length and meristem size in a
148 dose-dependent manner and to a similar extent (Fig S1H-J). Since cytokinins
149 determine root meristem size by controlling cell differentiation (Dello Iorio et al. 2007),

150 we checked the response of cytokinin-sensitive reporter line *TCS:GFP* in the primary
151 root apex, which showed highest expression in the columella and lateral root cap and
152 slight but significant repression under ammonium, revealing that cytokinin signaling
153 was not enhanced by ammonium (Bielach et al., 2012; Fig S2A, B). The histidine
154 kinase AHK3 acts as a cytokinin receptor to stimulate a two-component signaling
155 pathway that transfers a phosphorelay signal to the nucleus, where transcription
156 factors of the type-B ARABIDOPSIS RESPONSE REGULATOR gene family (ARR-B)
157 are activated (Ferreira and Kieber, 2005). We therefore examined ammonium
158 sensitivity via measuring primary root length and meristem size in the *ahk3-3*, *arr1-3*
159 and *arr12-1* mutants, which however revealed no difference to the wild-type (Fig
160 S2C-F), indicating that the AHK3/ARR1 and AHK3/ARR12 two-component cytokinin
161 signaling pathway was not targeted by ammonium. SHY/IAA3 acts directly
162 downstream of ARR1 and ARR12, which increases cell differentiation rate and
163 balances root-meristem size at the transition zone (Dello Iorio et al. 2008). However,
164 neither the *SHY2* deletion line *shy2-31* nor *shy2-2*, which expresses a stabilized
165 proteoform of SHY2 (Tian et al., 2002), exhibited altered ammonium sensitivity of
166 primary root elongation or meristem formation (Fig S2G-J). Taken together, these
167 observations indicated that cytokinin signaling is not involved in ammonium-
168 dependent inhibition of root elongation.

169
170 As ammonium has been reported to enhance ROS levels in plants (Patterson *et al.*,
171 2010; Xie *et al.*, 2015), we stained H₂O₂ in primary roots by 3,3'-diaminobenzidine
172 (DAB). Compared with nitrate, increasing ammonium supply gradually enhanced
173 repression of cell length and meristem size with the detection of H₂O₂ particularly in
174 the elongation and differentiation zones of the root apex (Fig 1A-G). Since nitrate-
175 supplied plants also showed similar DAB staining as ammonium-exposed plants in
176 the meristematic root zone, this zone was not considered as a primary target of
177 ammonium-induced ROS production. To better understand the source of ammonium-
178 dependent ROS formation in primary roots, we employed a pharmacological
179 approach and first applied potassium iodide (KI), acting as a chemical H₂O₂
180 scavenger (Lee *et al.*, 2013). KI largely reverted the ammonium-dependent inhibition
181 of the primary root elongation rate and restored cell length and meristem size to a
182 large extent (Fig 1A-F). Recovered root elongation coincided with lower abundance
183 of DAB-stained ROS in the elongation and differentiation zone of the primary root

184 (Fig 1G), suggesting that enhanced levels of H₂O₂ are responsible for the stunted
185 root phenotype. When ammonium-grown roots were exposed to elevated H₂O₂ levels,
186 which were generated either directly by supply of 1 mM H₂O₂ or indirectly by supply
187 of the peroxidase inhibitor salicylhydroxamic acid (SHAM), primary root elongation
188 rates declined drastically due to strongly decreased cell length and meristem size,
189 going along with enhanced DAB staining (Fig S3A-G). Notably, in nitrate-supplied
190 roots, meristem size and DAB staining were apparently not affected by H₂O₂ or
191 SHAM, while cortical cell length was only slightly decreased (Fig S3D-G), relating to
192 the fact that nitrate-supplied plants possess elevated ROS scavenging capacities
193 (Chu et al., 2021). To distinguish between the contribution of superoxide radicals
194 (O₂^{•-}) and H₂O₂, we investigated the effects of sodium diethyldithiocarbamate (DDC),
195 an inhibitor of Cu,Zn-superoxide dismutase (SOD) that blocks H₂O₂ generation and
196 leads to O₂^{•-} accumulation (Auh and Murphy, 1995). Both cell length and meristem
197 size of the primary root apex were partially but significantly rescued by DDC
198 supplementation, allowing partial recovery of primary root elongation (Fig S4). This
199 observation indicated that O₂^{•-} radicals are not the direct cause for ammonium-
200 mediated inhibition of root elongation, whereas SOD-catalyzed conversion of O₂^{•-} to
201 H₂O₂ matters. Alternatively, we suspected RBOH-type NADPH oxidases produce
202 ammonium-dependent ROS and examined a couple of *rboh* single or multiple knock-
203 out lines. However, none of them showed an ammonium-dependent root phenotype
204 (Fig S5).

205 Since in the absence of ammonium H₂O₂ was less effective in inhibiting root
206 elongation (Fig S3), we assumed ammonium-facilitated formation of H₂O₂ plays a
207 role and speculated that this process depends on the availability of Fe (Dixon and
208 Stockwell, 2014). Indeed, lowering Fe supply from 100 μM to 10 μM Fe(III)-EDTA
209 resulted in weaker inhibition of cell length, meristem size and primary root elongation
210 and prevented accumulation of DAB-stained ROS in the elongation and
211 differentiation zone of the primary root (Fig 1A-G). Higher resolution of DAB-stained
212 cells allowed assigning H₂O₂ to the stele of the late elongation and early
213 differentiation zone, which became shorter under increasing ammonium supply and
214 thus appeared more apical (Fig 2A). In addition, we localized ROS-dependent
215 fluorescence by the cell-permeant indicator 2',7'-dichlorofluorescein diacetate
216 (H₂DCFDA), revealing enhanced ROS formation in the stele, especially along the
217 vascular strands of ammonium-exposed roots with a maximum at the transition of the

218 elongation to the differentiation zone (Fig 2B, C). Considering Fe dependency of
219 ammonium-triggered root inhibition (Fig 1), Fe distribution in the root was stained by
220 DAB-enhanced Perls detecting both free Fe(II) and Fe(III) (Roschztardt et al., 2009).
221 While nitrate-grown roots accumulated some Fe in the meristematic zone,
222 ammonium-exposed roots showed much higher Fe accumulation especially in the
223 differentiation zone (Fig 2D). Cross sections of Perls/DAB-stained primary roots
224 showed that ammonium-dependent Fe precipitation was restricted by the Casparian
225 band and thus confined to the apoplast of outer root cells (Fig S6). Since Fe
226 availability increases with decreasing pH and ammonium nutrition is known to acidify
227 the rhizosphere and apoplast (Römheld and Marschner, 1986; Meier et al., 2020),
228 apoplastic pH changes were traced by using the apo-pHusion line, a ratiometric
229 reporter of apoplastic pH (Gjetting et al., 2012). Increasing ammonium nutrition
230 decreased apoplastic pH in particular in the elongation and differentiation zone of
231 ammonium-exposed roots (Fig 2E, F), which co-localized with DAB- or fluorescence-
232 stained ROS (Fig 2A-D), suggesting that the ammonium-dependent pH decrease and
233 enhanced Fe availability caused ROS formation.

234 Since ammonium-induced repression of root elongation appears to be a rapid
235 response detected even 1 d after ammonium exposure (Fig S1E-G), we investigated
236 dynamic changes in Fe availability and ROS status in ammonium-supplied primary
237 roots. Enhanced Fe precipitation and ROS accumulation appeared as early as 1 d
238 after ammonium supply in the differentiation zone of the primary root and progressed
239 in the apical direction with time and in dependence of external ammonium supply (Fig
240 S7). As indicated by the arrows marking the boundaries of the meristematic and
241 elongation zones, the size of the elongation zone started declining earlier than that of
242 the meristematic zone, which went along with progression of H₂DCFDA-dependent
243 fluorescence into the elongation zone towards the meristematic zone (Fig 2B; S7B).
244 To verify an impact of ROS on cell division, we evaluated the response to ammonium
245 of the cell cycle reporter *CycB1;1::GUS* (Colón-Carmona et al., 1999). Ammonium
246 supply significantly suppressed GUS activity in the apical meristem of primary root,
247 and this suppression was largely alleviated by lowering external Fe supply (Fig S8).
248 Consistent with the decrease of meristem size and cell length under the same
249 conditions (Fig 1D-F), we conclude that Fe-dependent ROS formation is a major
250 repressor of both cell elongation and cell division in ammonium-exposed root apices.
251 Notably, exactly the same responses of apoplastic pH, Fe availability and ROS

252 formation as in primary root were detected in the apex of lateral roots (Fig S9),
253 indicating that oxidative stress acts as a common inhibitory mechanism underlying
254 ammonium-induced growth repression in both primary and lateral roots.

255 To manipulate Fe availability in the presence of ammonium, medium pH was
256 buffered at different values (Fig S10). While ammonium-inhibited root elongation was
257 aggravated when roots were shifted from standard pH 5.7 to pH 5.0, higher pH
258 restored root elongation leading to almost similar length of nitrate- and ammonium-
259 grown roots at pH 7.2 (Fig 3A-C). After 6 d of ammonium exposure, Perls/DAB
260 staining revealed decreasing Fe accumulation in the apical root zone with increasing
261 pH, except for the columella cells (Fig 3D). In contrast, strongly enhanced amounts of
262 Fe accumulated at pH 5.0 but only in ammonium-exposed roots. Since the pH of the
263 agar medium was buffered by MES, we suspected that buffer strength might affect
264 ammonium-induced pH changes and Fe availability under ammonium supply. Indeed,
265 lowering MES concentration from 2.5 to 0.5 mM dramatically aggravated Fe
266 precipitation and inhibition of ammonium-exposed primary root tips, while at 10 mM
267 MES Fe precipitation decreased and ammonium-repressed root elongation was
268 partially attenuated (Fig S11). These results indicated that the intensity of
269 ammonium-dependent proton release and acidification of the rhizosphere is of
270 immediate relevance for Fe mobilization and precipitation in the root apoplast and at
271 the root surface.

272
273 The dependence of ammonium-induced root growth inhibition on Fe recalls the role
274 of Fe in root growth inhibition under phosphate deficiency that also relies on Fe-
275 facilitated ROS formation (Müller et al., 2015). Recently, it has been reported that this
276 role of Fe represents a side effect of light exposure when roots are grown in
277 transparent Petri dishes (Zheng et al., 2019). Thus, we shaded the whole root system
278 by aluminium foil as described in Zheng et al. (2019) and noted that in all N
279 treatments primary root length increased when roots were shaded from white light
280 (Fig S12A, B). Even though ammonium-dependent primary root growth inhibition was
281 slightly alleviated by shielding roots from light, ammonium supply still arrested
282 primary root elongation to a large extent (Fig S12B, C). This observation supported
283 that light increases the pool of redox-active Fe (Zheng et al., 2019), which in the
284 presence of ammonium may engage in ROS formation and inhibit primary root
285 elongation.

286 Previous work under phosphate deficiency showed that blue light exposure
287 promotes the Fenton reaction converting H₂O₂ to hydroxyl radicals that are more
288 toxic oxygen species and strongly suppress primary root elongation (Zheng et al.,
289 2019). Here, to evaluate the involvement of hydroxyl radicals in ammonium-
290 dependent root growth inhibition, we supplied thiourea, a chemical scavenger of
291 hydroxyl radicals (Wasil et al., 1987), together with ammonium to the medium.
292 However, the presence of thiourea hardly altered the sensitivity of primary roots to
293 ammonium (Fig S13), indicating that the formation of hydroxyl radicals via the Fenton
294 reaction is not critical for ammonium-dependent root growth inhibition.

295

296 **Hypersensitivity of root elongation to ammonium relates to vitamin B₆** 297 **deficiency**

298 To explore how plants cope with ammonium-induced H₂O₂ formation and subsequent
299 root growth inhibition, we searched in publicly available transcriptome data for
300 ammonium-responsive genes that are expressed in roots (Patterson *et al.*, 2010;
301 Ristova *et al.*, 2016). We then collected T-DNA insertion lines of 29 ammonium-
302 responsive genes and screened them for primary root length under ammonium
303 versus nitrate supply (Data Set S1). In this screen, we identified a T-DNA insertion
304 line of *PDX1.1* (*SALK_024245*), which was hypersensitive to ammonium treatment
305 (Fig S14A, B). In Arabidopsis, PDX1.1 (along with PDX2) catalyzes vitamin B₆
306 biosynthesis *de novo* (Tambasco-Studart *et al.*, 2005; Fig S15), thus *pdx1.1* mutants
307 suffer from vitamin B₆ deficiency (Titiz *et al.*, 2006; Wagner *et al.*, 2006; Boycheva *et*
308 *al.*, 2015). We confirmed the hypersensitive phenotype of *pdx1.1* mutants to
309 ammonium by examining primary root growth in *SALK_024245* and the transposon
310 insertion line *pdx1.1-1* (Figure S14C-E). Since *SALK_024245* and *pdx1.1-1* showed
311 the same growth phenotype under ammonium supply in all our experiments, we
312 focused in the following on *SALK_024245*, naming it *pdx1.1-3*. Given that under
313 nitrate supply primary root growth of *pdx1.1-3* was weaker (Fig 4A), we calculated the
314 relative primary root elongation rate by normalizing it to the root growth rate under
315 nitrate. An earlier and steeper decrease in root elongation rate of *pdx1.1-3* than of
316 the wild type confirmed hypersensitivity of *pdx1.1-3* to ammonium nutrition (Fig 4B,
317 C). The higher sensitivity of *pdx1.1-3* to ammonium went along with elevated
318 accumulation of H₂O₂ in ammonium-exposed primary root tips already 2 d after
319 transfer to ammonium (Fig 4D).

320 To confirm whether the hypersensitivity of *pdx1.1-3* to ammonium is due to the defect
321 in vitamin B₆ biosynthesis, we supplied vitamin B₆ in the form of pyridoxine to the
322 growth medium. While external supply of pyridoxine to nitrate-grown wild-type plants
323 had no effect, it largely alleviated ammonium-induced inhibition of primary root
324 growth in the wild type and particularly in the *pdx1.1-3* mutant (Fig 4A). Notably,
325 external supplementation of pyridoxine recovered completely the primary root
326 elongation rate of *pdx1.1-3* (Fig 4B-C), cortical cell length and meristem size (Fig S16)
327 as well as GUS activity of the *CycB1;1::GUS* reporter (Fig S17), confirming that the
328 hypersensitive phenotype of *pdx1.1-3* to ammonium is due to defective vitamin B₆
329 biosynthesis. Since external supply of pyridoxine reduced also the accumulation of
330 DAB-stained H₂O₂ in ammonium-treated primary roots of both lines (Fig 4E), we
331 conclude that vitamin B₆ alleviates ammonium toxicity either by suppressing H₂O₂
332 generation or by scavenging H₂O₂ in primary root tips.

333

334 **Non-phosphorylated forms of vitamin B₆ are critical for ammonium** 335 **detoxification**

336 Vitamin B₆ is essential for all living organisms, and refers to a group of six different
337 vitamers that contain a pyridine ring and include the non-phosphorylated forms
338 pyridoxal (PL), pyridoxine (PN) and pyridoxamine (PM), as well as the
339 phosphorylated forms pyridoxal 5'-phosphate (PLP), pyridoxine 5'-phosphate (PNP)
340 and pyridoxamine 5'-phosphate (PMP) (Fitzpatrick, 2011; Fig S15). To evaluate their
341 efficacy in mitigating root growth inhibition, we supplied different B₆ vitamers to the
342 medium. Compared with the mock treatment, external supply of PLP slightly retarded
343 the ceasing primary root elongation during the first 4 d after transfer to ammonium,
344 but it hardly restored primary root length after 6 d of ammonium supply (Fig S18A-C).
345 By contrast, exogenous application of the vitamin B₆ forms PL or PN effectively
346 rescued primary root growth under ammonium supply, even during later stages of the
347 treatment, indicating a superior efficacy of the non-phosphorylated B₆ vitamers.
348 When monitoring the H₂O₂ status in root tips in parallel with root elongation,
349 exogenous application of PN or PL but not of PLP quenched excess accumulation of
350 H₂O₂ in ammonium-treated primary root tips (Fig S18D). These results reveal that
351 mitigation of root growth inhibition refers to the non-phosphorylated forms of vitamin
352 B₆ and their ability to suppress H₂O₂ accumulation.

353

354 **Over-expression of *PDX1.1* improves ammonium tolerance in roots**

355 To address the question whether *PDX1.1* plays a role in eliminating ammonium-
356 triggered ROS, we inspected three independent *PDX1.1* overexpression lines
357 (Raschke *et al.*, 2011). All three lines continued elongating their primary roots even
358 after 6 d of ammonium exposure when root elongation of the wild- type was almost
359 completely exhausted (Fig 5A-C). DAB staining showed that overexpression of
360 *PDX1.1* strongly reduced the level of H₂O₂ in ammonium-treated primary roots (Fig
361 5D). Accordingly, ammonium-induced inhibition of root cortical cell length, meristem
362 size and activity of the *CycB1;1::GUS* reporter also recovered by overexpression of
363 *PDX1.1* (Fig 5E-G; Fig S19), revealing the efficacy of endogenous vitamin B₆
364 formation under ammonium nutrition. Moreover, an ¹⁵NH₄⁺ influx experiment revealed
365 that the ammonium uptake capacity in roots remained unaffected in the *pdx1.1-3*
366 mutant as well as in the *PDX1.1* overexpression lines (Fig 5H). Taken together,
367 elevated expression of *PDX1.1* is sufficient to restore elongation in ammonium-
368 exposed roots and acts downstream of the ammonium uptake process.

369

370 **Overexpression of *PDX1.1* increases the level of non-phosphorylated B₆** 371 **vitamers**

372 As the *PDX1*-dependent step in vitamin B₆ biosynthesis yields first PLP (Fig S15), we
373 hypothesized that overexpression of *PDX1.1* will primarily increase phosphorylated
374 rather than non-phosphorylated vitamers, whose generation requires an additional
375 phosphatase reaction. Measuring vitamin B₆ in roots confirmed significantly lower
376 levels of total vitamin B₆ in the *pdx1.1-3* mutant than in the wild type, which was
377 caused by a significant decrease in the concentrations of all five determined B₆
378 vitamers (Fig 6A, B). At first glance, this suggested a constitutive contribution of
379 *PDX1.1* to overall vitamin B₆ biosynthesis because vitamin B₆ levels decreased in
380 *pdx1.1-3* irrespective of the supplied N form. Overexpression of *PDX1.1* led to
381 constitutively higher total vitamin B₆ levels only in *PDX1.1OE-L5*, but under
382 ammonium supply also in *PDX1.1OE-L15* and to lesser extent in *PDX1.1OE-L8*,
383 which coincided with elevated *PDX1.1* transcript levels in these lines (Fig 6A-C).
384 Surprisingly, the concentration of PLP was not enhanced in ammonium-supplied
385 *PDX1.1* overexpression lines, although PLP contributed > 70% to overall vitamin B₆
386 levels. In contrast, *PDX1.1* overexpression lines showed significantly higher
387 concentrations of non-phosphorylated vitamin B₆ forms than the wild- type, and these

388 differences closely reflected the relative differences in transcript levels among the
389 three overexpression lines. Hence, the proportion of individual B₆ vitamers shifted
390 towards the non-phosphorylated vitamin B₆ forms, among which PL was the most
391 abundant form contributing up to 25% of total vitamin B₆ (Fig 6B). PM accounted only
392 for approx. 1% of total vitamin B₆ in roots. In wild-type roots, 20% of total vitamin B₆
393 was in non-phosphorylated forms, while in *pdx1.1-3* this proportion was less than
394 10%. In *PDX1.1* overexpression lines, between 30% and 40% of total vitamin B₆ was
395 converted into non-phosphorylated forms and this share even increased when plants
396 were grown in the presence of ammonium (Fig 6A, B). We finally correlated the levels
397 of individual B₆ vitamers with those of *PDX1.1* transcripts and revealed close
398 correlations for PN, PL, and PM, but not for PMP, whereas the correlation for PLP
399 was also significant although much weaker (Fig 6D). These results indicate that the
400 extent of *PDX1.1* upregulation by ammonium or by ectopic expression determines
401 primarily the abundance of non-phosphorylated B₆ vitamers without compromising
402 homeostasis of phosphorylated B₆ vitamers in roots.

403

404 **H₂O₂ triggers localized upregulation of *PDX1.1* under ammonium supply**

405 To investigate the transcriptional regulation of vitamin B₆ biosynthesis and
406 homeostasis by ammonium, the transcript levels of all known genes involved in
407 vitamin B₆ biosynthesis or metabolism were examined by quantitative real-time PCR
408 in roots grown under different N supply. Unexpectedly, *PDX1.1* turned out to be the
409 sole vitamin B₆-related gene that was significantly upregulated by ammonium (Fig
410 7A). Next, the tissue-specific expression pattern of *PDX1.1* was monitored in plants
411 expressing a *PDX1.1* promoter-GUS reporter construct (Boycheva *et al.*, 2015).
412 *PDX1.1* reporter activity was upregulated by ammonium supply in the root
413 vasculature, increasing from the elongation zone basipetally through the
414 differentiation zone (Fig 7B). As the reporter activity became stronger in the presence
415 of 10 mM ammonium, upregulation of *PDX1.1* expression apparently followed
416 ammonium supply in a dose-dependent manner (Fig 7A, B).

417 Since the spatial localization of *PDX1.1* expression and H₂O₂ accumulation
418 strongly overlapped in ammonium-treated roots (Fig 2A-B, 7B), the question arose
419 whether ammonium itself or H₂O₂ triggered the upregulation of *PDX1.1*. We thus
420 suppressed H₂O₂ levels in ammonium-exposed roots by supply of KI or by low Fe
421 and observed that *PDX1.1* reporter activity disappeared (Fig 7B). By contrast,

422 exogenous application of 1 mM H₂O₂ strongly enhanced the promoter activity of
423 *PDX1.1* in the root stele as well as in the apical root meristem, however only in the
424 presence of ammonium (Fig 7C). Therefore, H₂O₂ serves as a signal to upregulate
425 *PDX1.1* transcription upon ammonium nutrition and determine its restricted
426 expression in the stele.

427 Given that the change of pH upon ammonium exposure is the initial event to
428 trigger the Fe-dependent oxidative burst, we hypothesized that the transcriptional
429 response of *PDX1.1* to ammonium should be influenced by medium pH. Indeed,
430 when *pPDX1.1:GUS* reporter lines were shifted from pH 5.7 to 5.0, the upregulation
431 of *PDX1.1* was enhanced in the presence of ammonium. By contrast, when raising
432 medium pH from 5.7 to 6.5 or 7.2, the induction of *PDX1.1* by ammonium almost
433 disappeared (Fig S20). These findings confirmed that ammonium- and pH-dependent
434 H₂O₂ generation is required to induce the expression of *PDX1.1* in roots.

435

436 **Elevation of PDX1.1-mediated vitamin B₆ biosynthesis improves tolerance to** 437 **further nutrient-related stresses**

438 Apart from ammonium toxicity, other nutrient-related stresses also arrest root
439 elongation by elevated ROS formation, such as phosphate deficiency or nickel
440 toxicity (Müller *et al.*, 2015; Zheng *et al.*, 2019; Lesková *et al.*, 2020). We wondered
441 whether PDX1.1-mediated vitamin B₆ biosynthesis also counteracts these oxidative
442 stresses in plants. First, we inspected published transcriptome results (Bhosale *et al.*,
443 2018; Lesková *et al.*, 2020), to assess the response of vitamin B₆-related genes to
444 phosphate deficiency and nickel toxicity. Surprisingly, none of the known genes
445 involved in vitamin B₆ biosynthesis or metabolism, including *PDX1.1*, was
446 differentially expressed under phosphate deficiency or nickel toxicity (Fig S21A, B).
447 Next, the arrest of primary root elongation under phosphate deficiency or nickel
448 toxicity showed no difference between wild-type (Col-0) and *pdx1.1-3* mutant plants
449 (Fig S21C-F). These results suggested that vitamin B₆-dependent ROS protection did
450 not evolve as a strategy to alleviate oxidative stress in response to phosphate
451 deficiency or nickel toxicity in natural conditions. Nonetheless, coinciding with their
452 enhanced ROS scavenging capacity, all three *PDX1.1* overexpression lines exhibited
453 significantly improved root elongation under phosphate deficiency or nickel toxicity
454 (Fig S21C-F). This result suggests that enhanced *PDX1.1*-mediated vitamin B₆

455 biosynthesis can be applied as a practical strategy to improve the root tolerance to
456 multiple types of oxidative stress.

457

458 **DISCUSSION**

459 Application of ammonium-based N fertilizers in agricultural plant production bears the
460 risk of impaired root development when roots are exposed to ammonium-rich soil
461 patches (Britto and Kronzucker, 2002; Watt et al., 2006). Plants have evolved several
462 strategies to cope with the adverse effects of predominant ammonium nutrition, which
463 comprise enhanced N assimilation in roots (Cruz et al., 2005; Guan et al., 2016;
464 Konishi et al., 2017), ammonium compartmentalization to the apoplast or vacuole
465 (Loqué et al., 2005; Li et al., 2010; Bai et al., 2014), and activation of enzymatic
466 antioxidation systems to cope with ammonium-triggered ROS production (Patterson
467 et al., 2010; Xie et al., 2015). In this study, we describe the mechanistic basis
468 underlying ammonium-triggered ROS formation and identify with PDX1.1-dependent
469 vitamin B₆ synthesis a metabolic defense response to counteract ammonium-induced
470 ROS formation.

471

472 **Ammonium-dependent acidification triggers ROS formation via enhanced Fe** 473 **mobilization**

474 Ammonium toxicity belongs to one of several mineral element disorders that
475 associate root growth inhibition with the production of ROS (Fig 1; Xie et al., 2015).
476 Among those disorders, localization and generation of ROS differ in an element-
477 specific manner, pointing to different sources of ROS formation. For instance, root
478 growth inhibition by nickel has been related to ROS formation in outer cells of the
479 apical root zone (Leskova et al., 2020), while ROS accumulate predominantly in the
480 meristem and elongation zone under zinc deficiency (Nakayama et al. 2020) or in the
481 root vasculature from the meristematic through the elongation and differentiation
482 zone of salt-stressed plants (Jiang et al., 2012). Considering that experimental
483 visualization and localization of ROS depend not only on the site of generation but
484 also on chemical properties of the ROS-sensitive dye or reporter, we used here DAB
485 staining and H₂DCFDA-dependent fluorescence to localize ROS formation under
486 ammonium nutrition primarily to the vascular cylinder or stele in the elongation and
487 differentiation zones (Fig 2). With increasing ammonium supply and time of exposure
488 ROS formation gradually progressed through the elongation zone towards the

489 meristem (Fig 2B-C; S7B), where it coincided with suppressed cell length, meristem
490 size and cell division activity (Fig 1; S3; S8), revealing that the apical root meristem is
491 not the primary target of ammonium-dependent ROS generation especially at early
492 stages of ammonium exposure. Although cytokinins are crucial in balancing cell
493 division and meristem size (Dello Iorio et al., 2008), key components of cytokinin
494 signaling are apparently not involved in ammonium-dependent root growth inhibition
495 (Fig S2).

496 Since ammonium-dependent root growth inhibition was suppressed when H₂O₂
497 accumulation was chemically quenched by KI (Fig 1) but enhanced when H₂O₂
498 accumulation was favored in the presence of SHAM or by H₂O₂ supplementation (Fig
499 S3), H₂O₂ or a downstream product must have caused the stunted root phenotype.
500 This is supported by the observation that blocking H₂O₂ formation by DDC in favor of
501 O₂^{•-} accumulation prevented ammonium-dependent root growth inhibition (Fig S4).
502 On the other hand, high effectiveness of SOD inhibition by DDC implied that DAB-stained
503 H₂O₂ was generated via O₂^{•-}, which in turn may derive from peroxisomes and the
504 mitochondrial electron transport chain or from the activity of NADPH oxidases in the
505 plasma membrane (Smirnoff and Arnaud, 2018). By examining a limited number of
506 available *rboh* single or multiple knock-out lines, we could not find evidence for a role
507 of RBOH-type NADPH oxidases in ammonium-triggered root growth inhibition (Fig
508 S5), even though our assay also included the root stele-localized RBOHF, which
509 triggers vascular ROS formation upon salinity as a prerequisite for salt tolerance
510 (Jiang et al., 2012). Irrespective of the O₂^{•-} source, SOD-mediated dismutation of O₂^{•-}
511 to H₂O₂ consumes protons and is favored by low apoplastic pH (Smirnoff and Arnaud,
512 2018) that resulted here from ammonium uptake-induced proton secretion (Fig 2; Fig
513 7D; Meier et al., 2020). Suppressed DAB staining and mitigation of root growth
514 inhibition under low Fe supply (Fig 1) indicated a key role of Fe in H₂O₂ formation.
515 Indeed, exposure of ammonium-grown roots to light, which increases the pool of
516 redox-active Fe (Zheng et al., 2019), aggravated inhibition of root elongation (Fig
517 S12). Furthermore, redox-active Fe(III) likely arose from apoplastic acidification and
518 dissolution of apoplastic Fe pools (Fig S6; Zhu et al., 2018) as well as from UV-
519 dependent photooxidation of EDTA that sets chelated ferric Fe free (Hangarter and
520 Stasinopoulos, 1991). A similarly critical role of ferrous Fe in ROS-mediated root
521 growth inhibition is also known for primary root growth inhibition under phosphate
522 starvation (Müller et al., 2015; Zheng et al., 2019). In this context, exposure of P-

523 deficient roots to light favors reduction of ferric to ferrous Fe and subsequent Fe²⁺-
524 mediated formation of hydroxyl radicals via the Fenton reaction. DAB-stained H₂O₂
525 under P deficiency is confined to the meristematic root zone and further depends on
526 malate efflux via ALMT1 (Zheng et al., 2019) to increase Fe solubility in the apoplast
527 (Balzergue et al., 2017; Mora-Macías et al., 2017). Since the root elongation in
528 response to ammonium was not altered in *almt1* mutants (Fig S14A, B), root shading
529 restored root elongation only in part (Fig S12) and ammonium-dependent H₂O₂
530 mainly localized to the root stele above the meristematic zone (Fig 2), mechanisms
531 underlying ROS formation clearly differ between P-deficient and ammonium-exposed
532 roots. Moreover, supplementation of the hydroxyl radical scavenger thiourea, which
533 can restore arrested primary root elongation under P deficiency (Zheng et al., 2019),
534 was poorly effective in the case of ammonium (Fig S13), suggesting that formation of
535 hydroxyl radicals via the Fenton reaction is not critical for ammonium-dependent root
536 growth inhibition. Nonetheless, a determinant role of redox-active Fe in ammonium-
537 triggered root growth inhibition is corroborated by its gradual relief under increasing
538 medium pH, which also decreased Fe accumulation in the root and subsequent Fe
539 availability for ROS metabolism (Fig 3). We thus conclude that ammonium-induced
540 acidification of the root apoplast and additionally in the rhizosphere enhance Fe
541 solubilization as prerequisite for re-location to the stele and subsequent Fe-mediated
542 formation of H₂O₂.

543

544 **Plant roots counteract ammonium-induced ROS formation via PDX1.1-** 545 **mediated vitamin B₆ biosynthesis**

546 In plants, vitamin B₆ is synthesized via the “deoxyxylulose-5-phosphate (DXP)-
547 independent pathway”, which utilizes ribose-5-phosphate, glyceraldehyde-3-
548 phosphate and glutamine as substrates for the glutamine amidotransferase complex
549 comprised of pyridoxine synthase (PDX1) and pyridoxine glutaminase (PDX2)
550 (Tambasco-Studart et al., 2005). The primary product is the phosphorylated form
551 PLP (Tambasco-Studart et al., 2005) before enzymes of the salvage pathway
552 facilitate the interconversion among different B₆ vitamers (Colinas et al., 2016; Fig
553 S15). While PLP acts as coenzyme in numerous enzymatic reactions, including those
554 with importance for N assimilation (Percudani and Peracchi, 2003; Fitzpatrick, 2011;
555 Colinas *et al.*, 2016), non-phosphorylated forms of vitamin B₆ serve efficiently as
556 antioxidants *in vitro* and *in vivo* (Bilski et al., 2000; Havaux et al., 2009; Mooney and

557 Hellmann, 2010). Our study provides several lines of evidence indicating that plants
558 induce PDX1.1-mediated synthesis of non-phosphorylated B₆ vitamers as an efficient
559 strategy to counteract ammonium-dependent oxidative stress in roots.

560 First, as several enzymes are required for vitamin B₆ biosynthesis and homeostasis,
561 it was surprising that only one of them, *PDX1.1*, responded to ammonium with
562 enhanced expression (Fig 7A). Indeed, overexpression of *PDX1.1* suppressed
563 ammonium-dependent H₂O₂ formation and associated root length inhibition, whereas
564 *pdx1.1* mutant lines were hypersensitive to ammonium (Fig 4 and 5, Fig S14). As in
565 these lines total vitamin B₆ levels closely followed *PDX1.1* transcript levels in roots,
566 transcriptional regulation of PDX1.1-dependent PLP synthesis alone provides
567 sufficient plasticity to counteract the adverse growth effect of ammonium. Among the
568 three paralogs of PDX1 in Arabidopsis, only PDX1.1 and PDX1.3 show catalytic
569 activities (Tambasco-Studart et al., 2005), while *PDX1.2* encodes a pseudoenzyme
570 that can boost vitamin B₆ biosynthesis via heteromerization with its paralogs in
571 response to singlet oxygen or heat stress (Moccand et al., 2014). Although spatial
572 and temporal expression patterns of *PDX1.1* and *PDX1.3* largely overlap and only
573 disruption of both genes causes embryo lethality, PDX1.3 has been found to be more
574 abundant and requisite for stress tolerance than PDX1.1 (Titiz et al., 2006).
575 Nonetheless, enhanced expression of PDX1.3 at the protein level appears to require
576 PDX1.2 (Dell'Aglio et al., 2017), whereas overexpression of PDX1.1 can be achieved
577 with the protein alone to substantially increase vitamin B₆ production (Raschke et al.,
578 2011; Fig 6). This regulatory versatility of PDX1.1 may provide an advantage when
579 plants need to respond instantly to oxidative stresses.

580 Second, external supply of vitamin B₆ to *pdx1.1-3* mutant or wild-type plants
581 completely prevented ammonium-induced inhibition of root elongation (Fig 4).
582 Although the overall vitamin B₆ level in the *pdx1.1-3* mutant line was only 20-30%
583 lower than in the wild type (Fig 6A), this difference as well as a further 50-100%
584 increase in the overexpressing lines gradually improved root growth, indicating a
585 strong dose dependence of beneficial vitamin B₆ action. This dose-dependent effect
586 went back to the abundance of the non-phosphorylated B₆ vitamers (Fig 6A),
587 because only PL and PN restored root length while the primary biosynthesis product
588 PLP remained ineffective (Fig S18). Superior functionality of non-phosphorylated
589 vitamers as ROS scavengers is most likely determined by substituents of the
590 pyridoxine core that modulate electron density in the ring and thus the interaction with

591 singlet molecular oxygen ($^1\text{O}_2$; Bilski et al., 2000). Upon quenching of $^1\text{O}_2$ the
592 pyridoxine ring is degraded (Bilski et al., 2000), explaining the dose-dependent rather
593 than catalytic effect of vitamin B₆ as observed here (Fig 5, 6). Since in
594 overexpression lines root concentrations of the three non-phosphorylated vitamers
595 PM, PN and PL only, correlated closely with *PDX1.1* transcript levels (Fig 6D),
596 transcriptional upregulation of *PDX1.1* is sufficient to confer a B₆ vitamer-specific
597 defense response to stress.

598 Third, *PDX1.1*-mediated biosynthesis *de novo* of vitamin B₆ spatially and temporally
599 coincides with ammonium-induced ROS formation in roots. Within a time frame of a
600 few days, there was a robust temporal coincidence between root elongation rates
601 and H₂O₂ accumulation, even when vitamin B₆ was provided externally or *PDX1.1*
602 expression levels were modulated (Fig 4, 5). Also at the tissue level, spatial patterns
603 of *PDX1.1* transcript levels and H₂O₂ accumulation strongly overlapped in
604 ammonium-treated roots (Fig 2, 7), supporting the notion that vitamin B₆ biosynthesis
605 is targeted to those tissues and root developmental zones that are most severely
606 affected by ROS accumulation. In plants, biosynthesis *de novo* of vitamin B₆ relies on
607 PDX2 using glutamine as a substrate to produce PLP (Fig S15; Tambasco-Studart et
608 al., 2005; Fitzpatrick et al., 2007; Boycheva et al., 2015). Glutamine is also the most
609 abundant product of ammonium assimilation in roots (Xu et al., 2012; Liu and von
610 Wirén, 2017), which is mediated by cytosolic glutamine synthetase. Interestingly,
611 GLN1;2-mediated glutamine synthesis preferentially localizes in the root vasculature
612 and GLN1;2 represents the most strongly upregulated GLN isoform in ammonium-
613 supplied roots (Ishiyama et al., 2004; Lothier et al., 2011; Guan et al., 2016).
614 Alternatively, ammonium may also be used directly by PDX1.1, independently of
615 PDX2 action, as has been demonstrated *in vitro* (Raschle et al., 2007). In this context,
616 elevated availability not only of glutamine but also of ammonium as one educt for
617 vitamin B₆ synthesis in those cells that suffer most from ROS production may be a
618 factor why plants favored vitamin B₆ as preferential ROS scavenger during
619 evolutionary adaptation to elevated external ammonium levels. Given that
620 ammonium-induced ROS formation occurs in all the cell types of the root
621 differentiation zone and meristem (Fig 2A-C; S7B) while the enhancement of
622 PDX1.1-mediated vitamin B₆ biosynthesis under ammonium supply is confined to the
623 vasculature (Fig 7B; S20), the question arises how root cells that do not produce
624 vitamin B₆ are protected from oxidative stress. Likely there is a radial transport

625 pathway bringing vitamin B₆ from the vasculature to the outer root cells, driven either
626 by diffusion of non-phosphorylated B₆ vitamers that are considered able to permeate
627 membranes (Stolz and Vielreicher, 2003), or by radial transport via membrane
628 proteins, such as purine permeases (PUPs). In particular PUP1 has been shown to
629 transport non-phosphorylated B₆ vitamers in Arabidopsis as well as after
630 heterologous expression in yeast (Szydlowski et al., 2013).

631
632 Vitamin B₆ has proven effective in ROS detoxification in a variety of systems and
633 conditions. In different human cell cultures, the supplementation of non-
634 phosphorylated forms of vitamin B₆ alleviates superoxide-induced damage and lipid
635 peroxidation (Jain and Lim, 2001; Kannan and Jain, 2004; Mahfouz et al., 2009). In
636 Arabidopsis protoplasts, PN supplementation can reduce oxidative damage
637 generated upon high illumination (Danon et al., 2005). When leaf discs were exposed
638 directly to ¹O₂, lipid peroxidation in the *pdx1.3* background was higher than in the wild
639 type (Havaux et al., 2009). Since this effect was not observed with O₂^{•-} or H₂O₂, and
640 since ¹O₂ levels rise during illumination more drastically in the *pdx1.3* mutant than in
641 the wild type, vitamin B₆ has been proposed to act as ¹O₂ quencher (Danon et al.,
642 2005; Havaux et al., 2009). Moreover, ¹O₂ can easily convert to O₂^{•-} by electron
643 transfer (Khan and Kasha, 1994) and is further converted to H₂O₂ by SOD, allowing
644 reactive Fe to take in a key role in ammonium-induced ROS processing (Fig 7D). Our
645 study could not identify the source of produced ¹O₂ or O₂^{•-} species, as analysis of a
646 few tested *rboh* mutants did not provide sufficient evidence to rule out NADPH
647 oxidases as a source for O₂^{•-} formation (Fig S5). Alternatively, ¹O₂ or O₂^{•-} species
648 may derive from electron transport processes in root plastids or mitochondria
649 (Smirnoff and Arnaud, 2018). Irrespective of their origin, their accumulation during
650 repression of SOD by DDC was ineffective in inhibiting root elongation (Fig S4),
651 indicating that the conversion of O₂^{•-} to H₂O₂ by SOD was required to inhibit root
652 elongation (Fig 7D). Actually, these two ROS species greatly influence root
653 development by regulating the balance between cell proliferation and cell
654 differentiation in the root tips (Tsukagoshi, 2016). Specifically, O₂^{•-} localized in the
655 meristematic zone maintains cell division, while H₂O₂ prevailing in the elongation
656 zone stimulates cell differentiation (Tsukagoshi et al., 2010). However, excessive
657 accumulation of H₂O₂ in the elongation zone leads to a repression of root growth
658 reflected by inhibited cell elongation and smaller meristem size (Tsukagoshi et al.,

659 2010). This may explain how H_2O_2 accumulation inhibited root elongation in
660 ammonium-grown plants (Fig 7D).

661 Based on our study, we propose a working model of the processes underlying
662 primary root growth inhibition under ammonium nutrition (Fig 7D). Ammonium uptake,
663 which is particularly high in the elongation zone (Duan et al., 2018), provokes
664 apoplastic acidification (Meier et al., 2020) that increases Fe solubilization and re-
665 precipitation in inner root cells (Fig 2, 7D). It is not yet completely clear why Fe
666 preferentially accumulates along the stele and whether the required change in Fe
667 binding forms for xylem loading is involved, but previous studies have confirmed
668 enhanced Fe precipitation in the pericycle and xylem (Green and Rogers, 2004;
669 Roschztardt et al., 2013). There, elevated Fe availability and acidic pH favor $O_2^{\cdot-}$
670 dismutation and H_2O_2 formation (Smirnov and Arnaud, 2018, Fig 7D). Considering that
671 ammonium uptake-dependent acidification stimulates the generation of H_2O_2 , H_2O_2
672 or a downstream product induces *PDX1.1* expression at the site of Fe and ROS
673 localization (Fig 7B, D). Predominant biosynthesis of non-phosphorylated B₆ vitamers
674 (Fig 6) can subsequently quench reactive molecular oxygen ($^1O_2/O_2^{\cdot-}$) that serves as
675 source for H_2O_2 formation (Fig S4) and thereby counteract ammonium-induced H_2O_2
676 formation to restore root growth. We find that this PDX1.1-mediated biosynthesis *de*
677 *novo* of vitamin B₆ is not only essential for protecting roots against ammonium toxicity,
678 as occurring in ammonium-enriched fertilizer bands in agricultural plant production,
679 but also effective against other adverse growth conditions that involve Fe-dependent
680 ROS formation such as P deficiency and nickel toxicity.

681

682

683 MATERIALS AND METHODS

684 Plant materials and growth conditions

685 *Arabidopsis thaliana* accession Col-0 and Ler served as wild type. The following
686 mutants and transgenic lines were used: *ahk3-3* (Dello loio et al., 2007), *arr1-3* (Dello
687 loio et al., 2007), *arr12-1* (Dello loio et al., 2007), *shy2-31* (Dello loio et al., 2008),
688 *shy2-2* (Dello loio et al., 2008), *TCS:GFP* (Bielach et al., 2012), *pdx1.1-1* (Titiz et al.,
689 2006), *pdx1.1-3* (SALK_024245), *apo-pHusion* (Gjetting et al., 2012), *PDX1.1OE-L5*
690 (Raschke et al., 2011), *PDX1.1OE-L8* (Raschke et al., 2011), *PDX1.1OE-L15*
691 (Raschke et al., 2011), *pPDX1.1:GUS* (Boycheva et al., 2015), *CycB1;1::GUS*
692 (Colón-Carmona et al., 1999). The cell cycle reporter *CycB1;1::GUS* (Col-0

693 background) was introduced into *pdx1.1-3* or *PDX1.10E-L5* by crossing to generate
694 *CycB1;1::GUS (pdx1.1-3)* and *CycB1;1::GUS (PDX1.10E-L5)* lines. Complete
695 information of T-DNA insertion lines of 29 ammonium-responsive genes used in the
696 mutagenesis screen are listed in Data Set S1. Arabidopsis seeds were surface
697 sterilized by 70% ethanol with 0.05% (v/v) Triton X-100, and cultured on modified
698 half-strength Murashige and Skoog (MS) medium containing 100 μM Fe(III)-EDTA,
699 0.5% sucrose, 1% Duchefa Phyto agar (Duchefa Biochemie), 2.5 mM MES pH 5.7,
700 and N sources were added to different final concentrations as described in the figure
701 legends. Seedlings grown in Petri dishes (12 x 12 cm) were cultured vertically in a
702 growth chamber under a 22°C/18°C and 10/14 h (light/dark) regime at the light
703 intensity of 120 $\mu\text{mol photons m}^{-2} \text{s}^{-1}$. For root phenotyping experiments, plants were
704 pre-cultured on half-strength MS medium containing 1 mM KNO_3 for 6 d, and then
705 transferred to treatment plates supplemented with half-strength MS medium
706 containing 1 mM KNO_3 , 1 mM NH_4Cl or 10 mM NH_4Cl respectively. 0.5 mM K_2SO_4
707 was added to balance K^+ concentration in the ammonium treatment. Root
708 phenotypes were measured 6 d after transfer. To generate P deficiency, 6 days-old
709 plants were transferred to half-strength MS medium containing 625 μM KH_2PO_4 (+P)
710 or 5 μM KH_2PO_4 (-P), KCl was added to -P medium to balance K^+ concentrations. For
711 Ni toxicity, 6 days-old plants were transferred to half-strength MS medium in the
712 absence (-Ni) or presence (+Ni) of 75 μM NiSO_4 . Root phenotypes were assessed 6
713 d after transfer. When supplementing H_2O_2 , fresh 30% H_2O_2 (Roth) solution (9.79 mol
714 L^{-1}) was diluted to a concentration of 1 M and supplied to the medium after
715 autoclaving. In the root shading experiment, root-containing segments of Petri dishes
716 were covered with aluminium foil as described in Zheng et al. (2019). For vitamin B_6
717 supplementation experiments, different B_6 vitamers were dissolved in water and
718 supplied to agar medium at a final concentration of 5 μM . Key chemical information is
719 given in Table S1.

720 **Root growth measurements**

721 During root phenotyping experiments, the position of primary roots was labeled every
722 day after treatment in order to calculate primary root elongation rate. Root images
723 were taken by an Epson 10000XL scanner at a resolution of 300 dpi. Primary root
724 growth parameters were measured by WinRHIZO Pro 2007 software (Regents
725 Instruments Canada). Differential interference contrast (DIC) microscopy images of
726 primary root tips were taken to assess the size of primary root meristem and the

727 length of mature cortical cell as described in Dello Iorio et al. (2007). All the
728 experiments were performed at least twice with similar results.

729 **ROS detection**

730 H₂O₂ in primary root tips were detected by 3,3'-Diaminobenzidine (DAB) staining as
731 described by Thordal-Christensen et al. (1997). Briefly, primary roots were incubated
732 in 1 mg ml⁻¹ DAB solution for 8 h, and then imaged by DIC microscopy. H₂O₂ is
733 visualized as a reddish-brown coloration. A cell-permeant fluorogenic dye 2',7'-
734 dichlorodihydrofluorescein diacetate (H₂DCFDA) was also used to measure ROS
735 activity in primary roots. Seedlings were stained for 20 min in a solution of 50 μM
736 H₂DCFDA in 50 mM potassium phosphate buffers (pH 7.0). DCF fluorescence was
737 excited at 488 nm and detected at 517-527 nm. Virtual color images were generated
738 by a rainbow color code to indicate the fluorescence intensity of DCF in roots.

739 **Apoplastic and rhizosphere pH measurements**

740 Apoplastic pH changes were measured by the ratiometric pH reporter apo-pHusion
741 (Gjetting et al., 2012). The fluorescence intensity ratio between pH-sensitive GFP
742 and pH-insensitive RFP was calculated to indicate the changes of apoplastic pH, and
743 virtual ratio images were generated by ImageJ v1.53 software. The changes of
744 rhizosphere pH under different N supply were monitored by the pH indicator
745 bromocresol purple (BCP) that changes color from yellow at pH 5.0 to violet at pH 7.2
746 (Meier et al., 2020). Six days after growth on different N sources, agar medium
747 containing six seedlings per plate were stained overnight (18 h) with BCP solution at
748 a final concentration of 0.1 mg ml⁻¹.

749 **Histological staining**

750 Promoter-driven β-glucuronidase (GUS) activity was determined by GUS staining as
751 described previously (Li, 2011). Roots were rinsed once with staining buffer
752 containing 50 mM NaHPO₄ buffer (pH 7.2), 2 mM potassium ferrocyanide, and 2 mM
753 potassium ferricyanide, and then incubated at 37°C in staining solution containing 2
754 mM X-Gluc. After staining, roots were cleared by HCG solution (chloral
755 hydrate:water:glycerol = 8:3:1) and imaged by DIC microscopy. To assess the size of
756 the primary root meristem and the length of mature cortical cell, non-staining primary
757 root tips were cleared by HCG solution and imaged by DIC microscopy. To stain Fe
758 accumulation in roots, a Perls staining and DAB/H₂O₂ intensification was performed
759 according to Roschztardt et al. (2009). Roots were rinsed three times with 10 mM
760 EDTA, and then incubated for 5 min in a freshly prepared Perls staining solution.

761 Afterward, roots were incubated in a methanol solution containing 0.01 M NaN₃ and
762 0.3% (v/v) H₂O₂ for 1 h at room temperature. After washing three times with 0.1 M
763 phosphate buffer (pH 7.4), roots were finally incubated for 5 min in an intensification
764 solution containing 0.025% (w/v) DAB and 0.005% (v/v) H₂O₂ in 0.1 M phosphate
765 buffer (pH 7.4). Roots were mounted with HCG solution before imaging by light
766 microscopy.

767 **Microscopy analyses**

768 Fluorescent images were taken by laser scanning confocal microscopy Zeiss LSM
769 780. Root samples were stained with 10 µg ml⁻¹ propidium iodide (PI) for 5 min to
770 visualize cell walls. GFP was excited at 488 nm and detected at 505-535 nm; RFP
771 was excited at 561 nm and detected at 580-630 nm; PI was excited at 561 nm and
772 detected at 600-700 nm. DCF fluorescence was excited at 488 nm and detected at
773 517-527 nm. The same microscope settings were kept to measure all confocal
774 sections across samples. Fluorescence quantification of apo-pHusion and H₂DCFDA
775 were conducted by Zeiss ZEN microscope software (version 2.6). Virtual ratio images
776 were generated by Image J 1.53 software. DAB staining, Perls staining, GUS staining
777 and DIC images were taken by Zeiss Axio Imager 2 system. For light microscopy of
778 *in situ*-localized Fe, root cuttings of 5 mm length of 5 seedlings from each growth
779 condition, were dissected approximately 1 cm above the root tip and subjected to
780 aldehyde fixation, dehydration and resin embedding as described in Table S2. Semi-
781 thin sections of 2.5 µm thickness were cut with a Leica UCT microtome (Leica
782 Microsystems, Wetzlar, Germany), and mounted on slides in rapid mounting medium
783 Entelan (Sigma-Aldrich, Darmstadt, Germany). Sections were recorded with a 40x
784 lense at fixed exposure time using a Zeiss Axio Imager M2 (Carl Zeiss Microscopy
785 GmbH, Oberkochen, Germany).

786

787 **Vitamin B₆ quantification analysis**

788 The abundance of all individual B₆ vitamers in roots were determined by HPLC.
789 Vitamin B₆ quantification analyses were performed as described previously (Colinas
790 et al., 2016) with the following changes: two separate extractions were performed
791 with 15 volumes and 8 volumes of 50 mM ammonium acetate (pH 4.0), respectively,
792 and a 50 µL injection volume was used for a single run per extract.

793 **Real-time quantitative PCR**

794 Total RNA was extracted from 10-20 mg frozen root samples by RNeasy plant mini
795 kit (Qiagen) following the manufacturer's protocol. Template cDNA was synthesized
796 from 1 µg total RNA using SuperScript II Reverse Transcriptase (Thermo Fisher
797 Scientific) and Oligo d(T)12-18 primer. Real-time qPCR was performed by CFX384
798 Touch Real-Time PCR Detection System (Bio-Rad) using iQ SYBR Green Supermix
799 (Bio-Rad). According to the multiple internal control method (Vandesompele et al.,
800 2002), relative transcript levels of target genes were calculated by the geNorm
801 algorithm (<https://genorm.cmgg.be>), using *UBQ10* (*AT4G05320*) and *ACTIN2*
802 (*AT3G18780*) as the multiple internal control genes in this study. Gene specific
803 primers for qPCR are listed in Table S3.

804 **Statistical analysis**

805 Data were collected and analyzed by Microsoft Excel 2016. Statistical analyses were
806 conducted by Graphpad Prism 8 (version 8.3.0). Two-tailed Student's *t*-test,
807 Dunnett's multiple test or Tukey's HSD test was performed to test the statistical
808 significance, and the *P*-value of each statistical analysis is described in the figure
809 legends. Graphs were plotted by Graphpad Prism 8 (version 8.3.0), and edited by
810 Adobe Illustrator 2020 (version 24.2.1).

811 **Accession numbers**

812 Sequence data in this study can be found in the Arabidopsis Information Resource
813 (TAIR) according to the following accession numbers: *PDX1.1* (*AT2G38230*), *PDX1.2*
814 (*AT3G16050*), *PDX1.3* (*AT5G01410*), *PDX2* (*AT5G60540*), *PDX3* (*AT5G49970*),
815 *SOS4* (*AT5G37850*), *PLR1* (*AT5G53580*), *UBQ10* (*AT4G05320*) and *ACTIN2*
816 (*AT3G18780*).

817

818 **AUTHOR CONTRIBUTIONS**

819 Y.L. and N. v. W. conceived the project and designed the experiments. Y.L., R.F.H.G.,
820 R.A.M., M.M., P.S. and T.B.F. performed the experiments and analyzed the data.
821 G.K. provided the transcriptome data. Y.L. and N.v.W. wrote the manuscript with
822 support of R.F.H.G. and T.B.F.

823

824 **ACKNOWLEDGMENTS**

825 We thank Twan Rutten (IPK Gatersleben) for microscopy advice. We thank Markus
826 Meier, Cevza Esin Tunc, and Mohammad-Reza Hajirezaei (IPK Gatersleben) for
827 scientific advice and valuable discussions. We further thank Jacqueline Fuge, Annett

828 Bieber, Elis Fraust, Barbara Kettig, Yudelsy Antonia Tandron Moya, Dagmar Böhmert
 829 and Christine Bethmann (IPK Gatersleben) for excellent technical assistance. This
 830 work was supported by the Deutsche Forschungsgemeinschaft (DFG, Germany) with
 831 a grant (WI1728/13-2) to N.v.W. The Swiss National Science Foundation is also
 832 acknowledged for funding to T.B.F. (grants 31003A_14117 and IZLIZ3_183193).

833

834 **FIGURE LEGENDS**

835 **Figure 1. Involvement of H₂O₂ and Fe in ammonium-dependent root growth**
 836 **inhibition.**

837 **(A)** Root phenotype of wild-type plants 6 d after transfer to different N supply, which
 838 contained additionally either 0.5 mM potassium iodide (KI) or 10 μ M Fe(III)-EDTA
 839 (low Fe) instead of 100 μ M Fe(III)-EDTA as in control plates. Horizontal marks along
 840 the root axis indicate daily positions of primary root tips. Root images were scanned 6
 841 d after transfer. Scale bar = 1 cm. **(B) - (C)** Relative primary root elongation rate
 842 under 1 mM ammonium supply **(B)** or under 10 mM ammonium supply **(C)**,
 843 normalized to the growth rate of plants treated with 1 mM nitrate. Symbols represent
 844 means \pm SE, n = 20 plants per treatment. Asterisks denote significant differences
 845 between control and indicated treatments at each time point as * $P < 0.05$ ** $P < 0.01$
 846 *** $P < 0.001$ according to Dunnett's multiple test. **(D)** Cell length and meristem size of
 847 primary roots. The length of mature cortical cells and the size of the root apical
 848 meristem are indicated by yellow arrowheads. DIC images of primary root tips were
 849 taken at 6 d after transfer. Scale bar = 100 μ m. **(E) - (F)** Quantitative readout of
 850 mature cortical cell length **(E)**, and primary root meristem size **(F)**. Boxes show the
 851 first quartile, median and third quartile; the whiskers show the minimum and
 852 maximum values, n = 16 plants. Different letters represent significant differences
 853 between treatments according to two-way ANOVA followed by Tukey's HSD test,
 854 $P < 0.05$. **(G)** DAB staining of H₂O₂ in primary root tips at 6 d after treatment. The
 855 reddish-brown coloration indicates H₂O₂. Representative images from 10 plants per
 856 treatment are shown. Scale bar = 200 μ m.

857 **Figure 2. Ammonium-dependent histochemical changes in the primary root**
 858 **apex.**

859 **(A)** DAB staining of H₂O₂ in primary root tips at 6 d after treatment. The reddish-
 860 brown coloration indicates H₂O₂. Representative images from 10 plants per treatment
 861 are shown. Scale bar = 100 μ m. **(B)** Staining of ROS (oxidant levels) by H₂DCFDA

862 staining. Rainbow color code (black to white) indicates DCF fluorescence intensity
 863 (low to high). Scale bars: 100 μm . **(C)** Quantitative readout of the fluorescence
 864 intensity of H₂DCFDA staining in different zones of the primary root. The boxes show
 865 the first quartile, median and third quartile; the whiskers show the minimum and
 866 maximum values. $n = 10$ independent plants. Different letters represent significant
 867 differences within each individual root zone at $P < 0.05$ according to Tukey's HSD test.
 868 **(D)** Perls/DAB staining of Fe as indicated by a reddish-brown color. Scale bars: 100
 869 μm . **(E)** Activity of the apoplastic pH sensor apo-pHusion. Color code (black to white)
 870 indicates fluorescence intensity ratio of eGFP/mRFP1 (low to high) and thus
 871 apoplastic pH. Scale bars: 100 μm . **(F)** Quantitative readout of the intensity ratio of
 872 eGFP/mRFP in different developmental zones of the primary root. Boxes show the
 873 first quartile, median and third quartile; the whiskers show the minimum and
 874 maximum values; $n = 10$ independent plants. Different letters represent significant
 875 differences within each individual root zone at $P < 0.05$ according to Tukey's HSD test.
 876 After a pre-culture of 6 d, wild-type or apo-pHusion plants were transferred to the
 877 treatment medium supplied with differing N forms. Histological staining and
 878 fluorescent imaging were performed 6 d after treatment. Representative images from
 879 10 plants per treatment are shown. Yellow arrowheads in **(A)** and **(D)**, or white
 880 arrowheads in **(B)** and **(E)**, indicate the boundaries of the meristematic zone,
 881 elongation zone and differentiation zone along the primary root.

882 **Figure 3. Influence of medium pH on primary root growth and root tissue Fe.**

883 **(A)** Root phenotype of wild-type plants 6 d after transfer to different N supply buffered
 884 at different pH. Medium pH of 5.0, 5.7 and 6.5 was buffered by 2.5 mM MES, while
 885 pH 7.2 was buffered by 2.5 mM MOPS. Horizontal marks along the root axis indicate
 886 daily positions of primary root tips. Scale bar = 1 cm. **(B) - (C)** Relative primary root
 887 elongation rate under 1 mM ammonium supply **(B)** or under 10 mM ammonium
 888 supply **(C)**, normalized to the growth rate of plants treated with 1 mM nitrate. Symbols
 889 represent means \pm SE, $n = 20$ plants per treatment. Asterisks denote significant
 890 differences between control (pH 5.7) and indicated treatments at each time point as *
 891 $P < 0.05$ ** $P < 0.01$ *** $P < 0.001$ according to Dunnett's multiple test. **(D)** Perls/DAB
 892 staining of Fe as indicated by a reddish-brown color. Perls/DAB staining was
 893 conducted at 6 d after transfer. Representative images from 10 plants per treatment
 894 are shown. Scale bars: 100 μm .

895 **Figure 4. Exogenous application of vitamin B₆ alleviates ammonium toxicity in**
 896 **roots.**

897 **(A)** Root phenotype of Col-0 and *pdx1.1-3* mutant plants 6 d after transfer to different
 898 N supply in the absence or presence of 5 μ M vitamin B₆ (pyridoxine). Horizontal
 899 marks along the root axis indicate daily positions of primary root tips. Scale bar = 1
 900 cm. **(B) - (C)** Relative primary root elongation rate under 1 mM ammonium supply **(B)**
 901 or under 10 mM ammonium supply **(C)**, normalized to the growth rate of plants
 902 treated with 1 mM nitrate. Data represent means \pm SE, n = 20 plants per treatment.
 903 Different letters represent significant differences at each time point at $P < 0.05$
 904 according to Tukey's HSD test. **(D)** H₂O₂ accumulation in the primary root as
 905 visualized by DAB staining in wild-type and *pdx1.1-3* mutant plants under differing N
 906 supply. DAB staining was conducted 2 d after treatment (2DAT) or 6 d after treatment
 907 (6DAT). Representative images from 10 seedlings per treatment are shown. Scale
 908 bar = 200 μ m. **(E)** DAB staining of H₂O₂ in primary root tips 6 d after treatment. The
 909 reddish-brown coloration indicates H₂O₂. Representative images from 10 seedlings
 910 per treatment are shown. Scale bar = 200 μ m.

911 **Figure 5. Over-expression of PDX1.1 enhances ammonium tolerance in roots.**

912 **(A)** Root phenotype of wild-type, *pdx1.1-3* mutant and three independent *PDX1.1*
 913 overexpression lines subjected to different N supply. Horizontal marks along the root
 914 axis indicate daily positions of primary root tips. After pre-culture of 6 d, plants were
 915 transferred to media containing different N forms. Root images were taken at 6 days
 916 after transfer. Scale bar = 1 cm. **(B) - (C)** Relative primary root elongation rate under
 917 1 mM ammonium supply **(B)** or under 10 mM ammonium supply **(C)**, normalized to
 918 the growth rate of plants treated with 1 mM nitrate. Symbols represent means \pm SE, n
 919 = 20 plants per treatment. Asterisks denote significant differences between wild type
 920 and indicated lines at each time point as * $P < 0.05$ ** $P < 0.01$ *** $P < 0.001$ by Dunnett's
 921 multiple test. **(D)** DAB staining of H₂O₂ in primary root tips of wild type, *pdx1.1-3* and
 922 *PDX1.1OE-L5* at 6 d after treatment. The reddish-brown coloration indicates H₂O₂.
 923 Representative images from 10 plants per treatment are shown. Scale bar = 200 μ m.
 924 **(E)** Cell length and meristem size of primary roots of wild type, *pdx1.1-3* and
 925 *PDX1.1OE-L5*. The length of mature cortical cells and the size of the root apical
 926 meristem are indicated by yellow arrowheads. DIC images of primary root tips were
 927 taken 6 d after treatment. Scale bar = 100 μ m. **(F) - (G)** Quantitative readout of
 928 mature cortical cell length **(F)**, and primary root meristem size **(G)**. Boxes show the

929 first quartile, median and third quartile; the whiskers show the minimum and
 930 maximum values, $n = 16$ plants. Different letters represent significant differences
 931 between lines and treatments according to two-way ANOVA followed by Tukey's
 932 HSD test, $P < 0.05$. **(H)** Influx of $^{15}\text{NH}_4^+$ into roots of wild type, *pdx1.1-3* mutant and
 933 *PDX1.1* overexpression lines. Plants were pre-cultured hydroponically for 5 weeks
 934 and then subjected to N starvation for 4 d before being transferred to $200 \mu\text{M}$ ^{15}N -
 935 labeled NH_4^+ for 6 min. Bars represent means \pm SD, $n = 5$ biological replicates.
 936 Asterisks denote significant differences between wild type and indicated lines at *
 937 $P < 0.05$ by Dunnett's multiple test; ns = not significant.

938 **Figure 6. Vitamin B₆ profiling of *pdx1.1* mutant and *PDX1.1*-overexpressing**
 939 **plants under different N regimes.**

940 **(A)** Root concentrations of vitamin B₆, pyridoxamine 5'-phosphate (PMP), pyridoxal
 941 5'-phosphate (PLP), pyridoxamine (PM), pyridoxine (PN) and pyridoxal (PL) in wild
 942 type (Col-0), *pdx1.1-3* mutant and three *PDX1.1* overexpression lines 6 d after
 943 transfer to different N supply. The amount of pyridoxine 5'-phosphate (PNP) was too
 944 low to be detected in this study. Bars represent means \pm SD, $n = 4$ independent
 945 biological replicates. Asterisks denote significant differences between wild type and
 946 indicated lines at * $P < 0.05$ ** $P < 0.01$ *** $P < 0.001$, by Dunnett's multiple test; ND =
 947 not detected. **(B)** Proportion of individual B₆ vitamers in the roots and **(C)** relative
 948 transcript abundance of *PDX1.1* in the roots of wild type, *pdx1.1-3* and *PDX1.1*
 949 overexpression lines 6 d after transfer to different N supplies. The relative transcript
 950 level of *PDX1.1* was determined by quantitative real-time PCR, and normalized by
 951 using *ACTIN2* and *UBQ10* as internal controls. Bars represent means \pm SD, $n = 4$
 952 independent biological replicates. **(D)** Correlation between the transcript abundance
 953 of *PDX1.1* and the concentration of individual B₆ vitamers in roots of wild type,
 954 *pdx1.1-3* and *PDX1.1* overexpression lines. Pearson's correlation coefficients are
 955 shown as R values.

956 **Figure 7. Transcriptional regulation of *PDX1.1* and other vitamin B₆-related**
 957 **genes in response to ammonium.**

958 **(A)** Relative transcript abundance of *PDX1.1*, *PDX1.2*, *PDX1.3*, *PDX2*, *PDX3*, *SOS4*
 959 and *PLR1* in roots of wild-type plants 6 d after transfer to different N supplies.
 960 Relative transcript levels were determined by quantitative real-time PCR and
 961 normalized by using both *ACTIN2* and *UBQ10* as multiple internal controls. Bars
 962 represent means \pm SD, $n = 3$ biological replicates. Different letters represent

963 significant differences among means at $P < 0.05$ according to Tukey's HSD test, ns =
964 not significant. **(B)** - **(C)** Promoter activity of the *pPDX1.1:GUS* reporter in primary
965 roots 6 d after transfer to different N treatments in the absence or presence of 0.5
966 mM KI or under supply of 10 μ M Fe(III)-EDTA (low Fe) **(B)** or in the presence of 1
967 mM H₂O₂ **(C)**. Representative images from 10 plants per treatment are shown. Scale
968 bar = 100 μ m. **(D)** Working model for the role of ammonium-triggered proton release
969 in Fe-dependent ROS metabolism and subsequent vitamin B₆ formation. Ammonium
970 uptake provokes proton secretion and apoplastic acidification which increases Fe
971 solubilization in the root apoplast and the rhizosphere along the elongation and
972 differentiation zones of the root. Secreted protons i) mobilize Fe from EDTA or the
973 apoplastic Fe pool (Fe(OH)₃), ii) enable superoxide dismutase (SOD)-mediated
974 conversion of superoxide (O₂^{•-}) to H₂O₂. H₂O₂ upregulates *PDX1.1* expression to
975 enhance accumulation of non-phosphorylated B₆ vitamers, in particular pyridoxine
976 (PN) and pyridoxal (PL), which serve as antioxidants quenching the reactive
977 molecular oxygen species ¹O₂ or O₂^{•-}. The root images on the right and left side refer
978 to the primary root tips of DAB-stained seedlings and *pPDX1.1:GUS* reporter lines
979 under ammonium supply, respectively.

980

981

982 **SUPPLEMENTAL FIGURE LEGENDS**983 **Figure S1. Ammonium suppresses root elongation in Arabidopsis.**

984 **(A)** Visual appearance of seedlings subjected to different N supplies. Wild-type plants
 985 were pre-cultured on half-strength MS medium containing 1 mM NO_3^- for 6 d before
 986 being transferred to 1 mM NO_3^- , 1 mM NH_4^+ or 10 mM NH_4^+ as sole N source. During
 987 plant growth, the positions of primary root tips were labeled every day to calculate
 988 primary root elongation rates. Images were taken 6 d after transfer. Scale bar = 1 cm.
 989 **(B) - (D)**, Primary root length **(B)**, total lateral root length **(C)**, and mean lateral root
 990 length **(D)** of wild-type plants 6 d after transfer to different N treatments. Boxes show
 991 the first quartile, median and third quartile; the whiskers show the minimum and
 992 maximum values, $n = 20$ independent plants. Different letters represent significant
 993 differences at $P < 0.05$ according to Tukey's HSD test. **(E) - (G)**, Primary root length
 994 **(E)**, primary root elongation rate **(F)**, and relative primary root elongation rate **(G)** of
 995 wild-type plants under differing N supplies. Symbols represent means \pm SE, $n = 20$
 996 plants per treatment. Different letters in **(E)** and **(F)** represent significant differences
 997 within each time point at $P < 0.05$ according to Tukey's HSD test. Different letters in **(G)**
 998 denote significant differences among time points under 1 mM or 10 mM NH_4^+
 999 respectively, according to Tukey's HSD test. **(H)** Cell length and meristem size of
 1000 primary roots. Primary roots were stained by propidium iodide (PI), and confocal
 1001 images were taken 6 d after transfer. The length of mature cortical cells and the size
 1002 of the root apical meristem are indicated by red arrowheads. Scale bar = 100 μm . **(I) -**
 1003 **(J)**, Quantitative readout of primary root meristem size **(I)**, and mature cortical cell
 1004 length **(J)**. Boxes show the first quartile, median and third quartile; the whiskers show
 1005 the minimum and maximum values, $n = 20$ plants. Different letters represent
 1006 significant differences at $P < 0.05$ according to Tukey's HSD test.

1007 **Figure S2. Cytokinin signaling is not involved in ammonium-dependent**
 1008 **inhibition of root growth.**

1009 **(A)** Expression pattern of the cytokinin reporter *TCS:GFP* in primary root tips under
 1010 different N supply. Images were taken 6 d after transfer. **(B)** Quantitative readout of
 1011 *TCS:GFP* fluorescence intensity in primary roots under different N supply. Boxes
 1012 show the first quartile, median and third quartile; the whiskers show minimum and
 1013 maximum values, $n = 10$ plants. Asterisks denote significant differences between wild
 1014 type and indicated lines at * $P < 0.05$ by two-tailed Student's *t*-test. **(C)** and **(G)**, Root
 1015 phenotype of wild-type (Col-0), *ahk3-3*, *arr1-3*, *arr12-1* mutants **(C)**, and wild-type

1016 (Ler), *shy2-31*, *shy2-2* mutants (**G**) subjected to different N supply. Roots were
 1017 scanned at 6 d after transfer. Scale bar = 1 cm. The position of primary root tips at
 1018 the day of transfer is labeled by black arrowheads. (**D**) and (**H**), Primary root length
 1019 after transfer of Col-0, *ahk3-3*, *arr1-3*, *arr12-1* (**D**), and Ler, *shy2-31*, *shy2-2* (**H**) to
 1020 different N supply. Boxes show the first quartile, median and third quartile; the
 1021 whiskers show the minimum and maximum values, n = 10 plants in (**D**), n = 12 plants
 1022 in (**H**). Different letters represent significant differences between treatments and lines
 1023 according to two-way ANOVA followed by Tukey's HSD test at $P < 0.05$. (**E**) and (**I**),
 1024 Primary root meristems of Col-0, *ahk3-3*, *arr1-3*, *arr12-1* (**E**), and Ler, *shy2-31*, *shy2-*
 1025 *2* (**I**) under different N supply. The size of the primary root meristem is indicated by
 1026 yellow arrowheads in the images. Root images were taken at 6 d after transfer to
 1027 indicated N sources. Scale bar = 100 μm . (**F**) and (**J**), Quantitative readout of the
 1028 primary root meristem size of Col-0, *ahk3-3*, *arr1-3*, *arr12-1* (**F**), and Ler, *shy2-31*,
 1029 *shy2-2* (**J**). Boxes show the first quartile, median and third quartile; the whiskers
 1030 show the minimum and maximum values, n = 10 plants in (**F**), n = 12 plants in (**J**).
 1031 Different letters represent significant differences between treatments and lines
 1032 according to two-way ANOVA followed by Tukey's HSD test at $P < 0.05$.

1033 **Figure S3. H₂O₂ aggravates root growth inhibition in the presence of**
 1034 **ammonium.**

1035 (**A**) Root phenotype of wild-type plants 6 d after transfer to different N supply, in the
 1036 absence or presence of either 1 mM H₂O₂ or 20 μM SHAM. Horizontal marks along
 1037 the root axis indicate daily positions of primary root tips. Root images were scanned 6
 1038 d after transfer. Scale bar = 1 cm. (**B**) - (**C**) Relative primary root elongation rate
 1039 under 1 mM ammonium supply (**B**) and under 10 mM ammonium supply (**C**),
 1040 normalized to the growth rate of plants treated with 1 mM nitrate. Symbols represent
 1041 means \pm SE, n = 20 plants per treatment. Asterisks denote significant differences
 1042 between control and indicated treatments at each time point as * $P < 0.05$ ** $P < 0.01$
 1043 *** $P < 0.001$ according to Dunnett's multiple test. (**D**) Cell length and meristem size of
 1044 primary roots. The length of mature cortical cells and the size of the root apical
 1045 meristem are indicated by yellow arrowheads. DIC images of primary root tips were
 1046 taken at 6 d after transfer. Scale bar = 100 μm . (**E**) - (**F**) Quantitative readout of
 1047 cortical cell length (**E**), and meristem size (**F**). Boxes show the first quartile, median
 1048 and third quartile; the whiskers show the minimum and maximum values, n = 16
 1049 plants. Different letters represent significant differences between samples according

1050 to two-way ANOVA followed by Tukey's HSD test at $P < 0.05$. **(G)** DAB staining of
1051 H_2O_2 in primary root tips at 6 d after treatment. The reddish-brown coloration
1052 indicates H_2O_2 . Representative images from 10 plants per treatment are shown.
1053 Scale bar = 200 μm .

1054 **Figure S4. Superoxide is not causal for ammonium-dependent root growth**
1055 **inhibition.**

1056 **(A)** Schematic diagram of ROS metabolism and inhibitor action. Sodium
1057 diethyldithiocarbamate (DDC) acts as an inhibitor of superoxide dismutase (SOD),
1058 potassium iodide (KI) acts as H_2O_2 scavenger, and salicylhydroxamic acid (SHAM) is
1059 a peroxidase inhibitor (Lee *et al.*, 2013). **(B)** Root phenotype of wild-type plants 6 d
1060 after transfer to different N supply in the absence or presence of 100 μM DDC.
1061 Horizontal marks along the root axis indicate daily positions of primary root tips.
1062 Scale bar = 1 cm. **(C) - (D)** Relative primary root elongation rate under 1 mM
1063 ammonium supply **(C)** and under 10 mM ammonium supply **(D)**, normalized to the
1064 growth rate of plants treated with 1 mM nitrate. Symbols represent means \pm SE, $n =$
1065 20 plants per treatment. Asterisks denote significant differences between control and
1066 DDC treatment at each time point according to two-tailed Student's *t*-test at ***
1067 $P < 0.001$. **(E)** Cell length and meristem size of primary roots. Primary roots were
1068 stained by propidium iodide, and confocal images were taken 6 d after transfer. The
1069 length of mature cortical cells and the size of the root apical meristem are indicated
1070 by red arrowheads. Scale bar = 100 μm . **(F) - (G)** Quantitative readout of cortical cell
1071 length **(F)**, and meristem size **(G)**. Boxes show the first quartile, median and third
1072 quartile; the whiskers show the minimum and maximum values, $n = 20$ plants.
1073 Different letters represent significant differences between samples according to two-
1074 way ANOVA followed by Tukey's HSD test at $P < 0.05$.

1075 **Figure S5. Screening of *rboh* mutants under different N supply.**

1076 **(A)** Root phenotypes of wild-type plants and single or multiple *rboh* mutants in
1077 response to different N supply. After a pre-culture of 6 d, seedlings were transferred
1078 to medium containing either 1 mM nitrate or 1 mM ammonium as sole N source.
1079 Horizontal marks along the root axis indicate daily positions of primary root tips.
1080 Images were taken 6 d after treatment. Scale bar = 1 cm. **(B)** Primary root length
1081 after transfer. Boxes show the first quartile, median and third quartile; the whiskers
1082 show the minimum and maximum values, $n = 18$ plants. Different letters represent

1083 significant differences between samples according to two-way ANOVA followed by
1084 Tukey's HSD test at $P < 0.05$.

1085 **Figure S6. Fe precipitation in the primary root under nitrate or ammonium**
1086 **supply.**

1087 After a pre-culture of 6 d, wild-type plants were transferred to the medium supplied
1088 with 1 mM nitrate, 1 mM ammonium or 10 mM ammonium. Perls/DAB stained roots
1089 were embedded in Spurr resin. Root cross-sections were obtained from the
1090 differentiation zone of primary roots. Fe precipitation in primary roots is indicated by a
1091 reddish-brown colour. Scale bars: 50 μm .

1092 **Figure S7. Dynamic changes of the Fe and ROS status in primary root tips**
1093 **under different N supply.**

1094 **(A)** Perls/DAB staining of Fe as indicated by a reddish-brown color. After a pre-
1095 culture of 6 d, wild type (Col-0) plants were transferred to the treatment medium
1096 supplied with differing N forms. Histological staining was performed at the indicated
1097 days after transfer (DAT). Scale bars: 100 μm . **(B)** ROS status (oxidant levels) in
1098 primary root tips as monitored by H_2DCFDA staining. DCF fluorescence was
1099 detected by confocal microscopy at the indicated time points. Rainbow color code
1100 (black to white) indicates DCF fluorescence intensity (low to high). Scale bars: 100
1101 μm . **(C)** Quantitative readout of the fluorescence intensity of H_2DCFDA staining. The
1102 boxes show the first quartile, median and third quartile; the whiskers show the
1103 minimum and maximum values, $n = 12$ plants. Different letters represent significant
1104 differences between samples at $P < 0.05$ according to Tukey's HSD test. Orange
1105 arrowheads in **(A)**, or white arrowheads in **(B)**, indicate the boundaries of the
1106 meristematic zone, elongation zone and differentiation zone along the primary root.

1107 **Figure S8. Fe aggravates ammonium-repressed cell division in roots.**

1108 **(A)** GUS activity in primary root tips of a *CycB1;1::GUS* reporter line. After a pre-
1109 culture of 6 d, *CycB1;1::GUS* reporter plants were transferred to treatment medium
1110 supplied with different N forms. The treatment medium contained 100 μM Fe(III)-
1111 EDTA (control) or 10 μM Fe(III)-EDTA (low Fe). Histological staining was performed
1112 6 d after transfer. Scale bar = 100 μm . **(B)** Quantitative readout of the dividing cell
1113 number in primary root tips of *CycB1;1::GUS* reporter line. Boxes show the first
1114 quartile, median and third quartile; the whiskers show the minimum and maximum
1115 values, $n = 12$ plants. Different letters represent significant differences between
1116 samples according to two-way ANOVA followed by Tukey's HSD test at $P < 0.05$.

1117 **Figure S9. Ammonium-dependent histochemical changes in the lateral root**
1118 **apex.**

1119 **(A)** Cell length and meristem size of lateral root. After a pre-culture of 6 d, wild type
1120 (Col-0) seedlings were transferred to the treatment medium supplied with different N
1121 forms. Six days after transfer, lateral roots were stained by propidium iodide and
1122 imaged by confocal microscopy. The length of mature cortical cells and the size of
1123 the meristem are indicated by red arrowheads. Scale bar = 100 μm . **(B) - (C)**,
1124 Quantitative readout of lateral root meristem size **(B)**, and lateral root cortical cell
1125 length **(C)**. Boxes show the first quartile, median and third quartile; the whiskers show
1126 the minimum and maximum values, $n = 20$ plants. Different letters represent
1127 significant differences at $P < 0.05$ according to Tukey's HSD test. **(D)** DAB staining of
1128 H_2O_2 in lateral root tips at 6 d after treatment. The reddish-brown coloration indicates
1129 H_2O_2 . Representative images from 10 plants per treatment are shown. Scale bar =
1130 100 μm . **(E)** Detection of ROS (oxidant levels) by H_2DCFDA staining. Rainbow color
1131 code (black to white) indicates DCF fluorescence intensity (low to high). Scale bars:
1132 100 μm . **(F)** Quantitative readout of the fluorescence intensity of H_2DCFDA staining
1133 in lateral roots. The boxes show the first quartile, median and third quartile; the
1134 whiskers show the minimum and maximum values. $n = 12$ plants. Different letters
1135 represent significant differences at $P < 0.05$ according to Tukey's HSD test. **(G)**
1136 Perls/DAB staining of Fe in lateral root tips as indicated by a reddish-brown color.
1137 Representative images from 10 plants per treatment are shown. Scale bars: 100 μm .
1138 **(H)** Activity of the apoplastic pH sensor apo-pHusion in lateral roots. Color code
1139 (black to white) indicates fluorescence intensity ratio of eGFP/mRFP1 (low to high)
1140 and thus apoplastic pH. Scale bars: 100 μm . **(I)** Quantitative readout of the intensity
1141 ratio of eGFP/mRFP in lateral root. Boxes show the first quartile, median and third
1142 quartile; the whiskers show the minimum and maximum values; $n = 12$ plants.
1143 Different letters represent significant differences at $P < 0.05$ according to Tukey's HSD
1144 test. Yellow arrowheads in **(D)** and **(G)**, or white arrowheads in **(E)** and **(H)**, indicate
1145 the boundaries of the meristematic and elongation zone along the lateral root.

1146 **Figure S10. Changes in rhizosphere pH after supply of different N forms.**

1147 After a pre-culture of 6 d, wild-type (Col-0) seedlings were transferred to the
1148 treatment medium supplied with different N forms. Medium pH of 5.0, 5.7 and 6.5
1149 was buffered by 2.5 mM MES, while pH 7.2 was buffered by 2.5 mM MOPS.
1150 Changes of medium pH through plants are monitored by the pH indicator

1151 bromocresol purple (BCP) that changes color from yellow at pH 5.0 to violet at pH 7.2,
1152 while the left side of the plates without plants serves as a blank.

1153 **Figure S11. Influence of buffer strength on root growth and root Fe status.**

1154 **(A)** Root phenotype of wild-type (Col-0) plants 6 d after transfer to treatment medium
1155 containing MES buffer at different strength. Horizontal marks along the root axis
1156 indicate daily positions of primary root tips. Scale bar = 1 cm. **(B)** - **(C)** Relative
1157 primary root elongation rate under supply of 1 mM ammonium **(B)** or 10 mM
1158 ammonium **(C)**, normalized to the growth rate of plants treated with 1 mM nitrate.
1159 Symbols represent means \pm SE, $n = 20$ plants per treatment. Asterisks denote
1160 significant differences between 2.5 mM MES and indicated treatments at each time
1161 point as * $P < 0.05$ ** $P < 0.01$ *** $P < 0.001$ according to Dunnett's multiple test. **(D)**
1162 Perls/DAB staining of Fe in primary root tips as indicated by a reddish-brown color.
1163 Perls/DAB staining was conducted at 6 d after transfer. Representative images from
1164 10 plants per treatment are shown. Scale bars: 100 μ m.

1165 **Figure S12. Light is not essential for ammonium-dependent inhibition of**
1166 **primary root elongation.**

1167 **(A)** Experimental setup of the root shading treatment. Petri dish-grown plants were
1168 exposed to white light in the control treatment (light), while the whole root zone was
1169 covered by aluminium foil in the shading treatment (shading), as described in Zheng
1170 et al. (2019). **(B)** Appearance of plants grown on the indicated nitrogen supply. After
1171 a pre-culture of 6 d, wild-type (Col-0) plants were transferred to the treatment plates
1172 and either exposed to light or shaded. Images were taken 6 d after transfer. Scale
1173 bar = 1 cm. **(C)** Primary root length after transfer of wild-type plants to light or
1174 shading. Boxes show the first quartile, median and third quartile; the whiskers show
1175 minimum and maximum values; $n = 20$ plants. Different letters represent significant
1176 differences at $P < 0.05$ according to Tukey's HSD test.

1177 **Figure S13. The formation of hydroxyl radicals is not critical for ammonium-**
1178 **inhibited root elongation.**

1179 **(A)** Root phenotype of wild-type (Col-0) plants 6 d after transfer to different N
1180 supplies in the absence (control) or presence of 0.5 mM or 1.0 mM thiourea.
1181 Horizontal marks along the root axis indicate daily positions of primary root tips.
1182 Scale bar = 1 cm. **(B)** - **(C)** Relative primary root elongation rate under supply of 1
1183 mM ammonium **(B)** or 10 mM ammonium **(C)**, normalized to the growth rate of plants
1184 treated with 1 mM nitrate. Symbols represent means \pm SE, $n = 20$ plants per
1185 treatment. Asterisks denote significant differences between control and thiourea

1186 treatments at each time point as * $P < 0.05$ ** $P < 0.01$ *** $P < 0.001$ according to
 1187 Dunnett's multiple test.

1188 **Figure S14. *pdx1.1* mutants are hypersensitive to ammonium.**

1189 **(A)** Phenotypic screening of T-DNA insertion lines of ammonium-responsive genes.
 1190 Primary root length under ammonium supply was taken as a read-out for ammonium
 1191 sensitivity. Candidate lines were pre-cultured on half-strength MS medium containing
 1192 1 mM nitrate for 6 d before being transferred to medium containing either 1 mM
 1193 nitrate or 1 mM ammonium as sole N source. Horizontal marks along the root axis
 1194 indicate daily positions of primary root tips. Images were taken 6 d after transfer.
 1195 Scale bar = 1 cm. **(B)** Relative primary root length after transfer to 1 mM ammonium,
 1196 normalized to the root length of plants treated with 1 mM nitrate. Asterisks denote
 1197 significant differences between wild-type (Col-0) and indicated lines as *** $P < 0.001$
 1198 according to by Dunnett's multiple test; ns = not significant. **(C)** Schematic diagram of
 1199 the T-DNA insertions in the *PDX1.1* gene. Positioning of the T-DNA insertion in
 1200 *pdx1.1-3* (SALK_024245) and the transposon insertion in *pdx1.1-1* (SM_3_22664)
 1201 (Titiz *et al.*, 2006). **(D)** Root phenotype of wild-type (Col-0), *pdx1.1-1* and *pdx1.1-3*
 1202 plants subjected to different N supplies. Horizontal marks along the root axis indicate
 1203 daily positions of primary root tips. Images were taken 6 d after transfer. Scale bar =
 1204 1 cm. **(E)** Primary root length of wild-type (Col-0) and *pdx1.1* mutant plants after
 1205 transfer to different N forms. Boxes show the first quartile, median and third quartile;
 1206 the whiskers show minimum and maximum values; n = 18 plants. Different letters
 1207 represent significant differences between samples according to two-way ANOVA
 1208 followed by Tukey's HSD test, $P < 0.05$.

1209 **Figure S15. Vitamin B₆ metabolism in Arabidopsis.**

1210 Vitamin B₆ comprises six different vitamers. PLP, as a phosphorylated B₆ vitamer is a
 1211 bioactive form participating as coenzyme in numerous enzymatic reactions. Non-
 1212 phosphorylated forms of vitamin B₆ are PN, PL, and PM. In plants, PLP is produced
 1213 by biosynthesis *de novo* (blue) or by the salvage pathway (brown) via the conversion
 1214 among different B₆ vitamers. This schematic is modified from Colinas *et al.* (2016).
 1215 Gln, glutamine; Glu, glutamate; R5P, ribose 5-phosphate; G3P, glyceraldehyde 3-
 1216 phosphate; PNP, pyridoxine 5'-phosphate; PLP, pyridoxal 5'-phosphate; PMP,
 1217 pyridoxamine 5'-phosphate; PN, pyridoxine; PL, pyridoxal; PM, pyridoxamine; P-ase,
 1218 phosphatase.

1219 **Figure S16. Exogenous application of vitamin B₆ rescues cell length and**
 1220 **meristem size under ammonium supply.**

1221 **(A) - (B)** Cell length and meristem size of primary roots of wild-type (Col-0) **(A)** or
 1222 *pdx1.1-3* mutant **(B)**. Plants grown under different N supply and in the absence (- VB₆)
 1223 or presence (+ VB₆) of 5 μM pyridoxine. DIC images of primary roots were taken 6 d
 1224 after transfer. The length of mature cortical cells and the size of the root apical
 1225 meristem are indicated by yellow arrowheads. Scale bar = 100 μm. **(C) - (D)**
 1226 Quantitative readout of cortical cell length **(C)**, and meristem size **(D)**. Boxes show
 1227 the first quartile, median and third quartile; the whiskers show the minimum and
 1228 maximum values, n = 16 plants. Different letters represent significant differences
 1229 between samples according to three-way ANOVA followed by Tukey's HSD test,
 1230 $P < 0.05$.

1231 **Figure S17. Exogenous application of vitamin B₆ restores cell division under**
 1232 **ammonium supply.**

1233 **(A)** GUS activity of the *CycB1;1::GUS* reporter in primary roots of wild-type (Col-0)
 1234 and *pdx1.1-3* mutant plants. After a pre-culture of 6 d, *CycB1;1::GUS* reporter lines
 1235 were transferred to different N forms in the absence (- VB₆) or presence (+ VB₆) of 5
 1236 μM pyridoxine. Histological staining were performed 6 d after treatment. Scale bar =
 1237 100 μm. **(B)** Quantitative readout of the number of dividing cells. Boxes show the first
 1238 quartile, median and third quartile; the whiskers show the minimum and maximum
 1239 values, n = 12 plants. Different letters represent significant differences among
 1240 treatments according to three-way ANOVA followed by Tukey's HSD test at $P < 0.05$.

1241 **Figure S18. Non-phosphorylated forms of vitamin B₆ are critical for ammonium**
 1242 **detoxification.**

1243 **(A)** Root phenotype of wild-type (Col-0) plants 6 d after transfer to different N supply
 1244 in the absence or presence of 5 μM vitamin B₆ provided either as pyridoxal 5'-
 1245 phosphate (PLP), pyridoxal (PL), or pyridoxine (PN). Horizontal marks along the root
 1246 axis indicate daily positions of primary root tips. Seedlings subjected to N supplies
 1247 with exogenous supplementation of different B₆ vitamers. Scale bar = 1 cm. **(B) - (C)**
 1248 Relative primary root elongation rate under 1 mM ammonium supply **(B)** or under 10
 1249 mM ammonium supply **(C)**, normalized to the growth rate of plants treated with 1 mM
 1250 nitrate. Symbols represent means ± SE, n = 20 plants per treatment. Asterisks
 1251 denote significant differences between control and indicated treatments at each time
 1252 point as * $P < 0.05$ ** $P < 0.01$ *** $P < 0.001$ according to Dunnett's multiple test. **(D)** DAB
 1253 staining of H₂O₂ in primary root tips 6 d after treatment. The reddish-brown coloration

1254 indicates H₂O₂. Representative images from 10 seedlings per treatment are shown.
1255 Scale bar = 200 μm.

1256 **Figure S19. Over-expression of *PDX1.1* rescues cell division under ammonium**
1257 **supply.**

1258 **(A)** GUS activity of the *CycB1;1::GUS* reporter in primary root tips of wild-type (Col-0),
1259 *pdx1.1-3* and *PDX1.1OE-L5* plants. After a pre-culture of 6 d, *CycB1;1::GUS* reporter
1260 lines were transferred to the treatment medium supplied with different N forms.
1261 Histological stainings were performed 6 d after transfer. Scale bar = 100 μm. **(B)**
1262 Quantitative readout of the number of dividing cells in primary root tips of
1263 *CycB1;1::GUS* reporter lines. Boxes show the first quartile, median and third quartile;
1264 the whiskers show the minimum and maximum values, n = 12 plants. Different letters
1265 represent significant differences between treatments and lines according to two-way
1266 ANOVA followed by Tukey's HSD test at *P*<0.05.

1267 **Figure S20. Influence of medium pH on the expression of *PDX1.1* upon**
1268 **ammonium supply.**

1269 Promoter activities of the *pPDX1.1::GUS* reporter in primary roots subjected to
1270 different N forms and buffered at different pH were monitored by GUS staining 6 d
1271 after transfer. Medium pH of 5.0, 5.7 and 6.5 was buffered by 2.5 mM MES, while pH
1272 7.2 was buffered by 2.5 mM MOPS. Representative images from 10 plants per
1273 treatment are shown. Scale bar = 100 μm.

1274 **Figure S21. Over-expression of *PDX1.1* improves tolerance to P deficiency and**
1275 **Ni toxicity.**

1276 **(A) - (B)** Heat map displaying the relative expression level of vitamin B₆-related
1277 genes (highlighted in boxes) in response to phosphorus deficiency **(A)** or nickel
1278 toxicity **(B)**. Data were retrieved from published microarray experiments (Bhosale et
1279 al., 2018; Lesková et al., 2020). Selected genes previously shown to be up- or down-
1280 regulated by phosphorus deficiency or nickel toxicity were included as controls. -P, 5
1281 μM phosphate; +P, 625 μM phosphate; ++Ni, 100 μM nickel; control, no nickel added
1282 to growth medium. **(C)** Appearance of plants grown on different phosphate (P)
1283 supplies. After a pre-culture of 6 d, the seedlings of Col-0, *pdx1.1-3*, *PDX1.1OE-L5*,
1284 *PDX1.1OE-L15* and *PDX1.1OE-L8* were transferred to treatment medium containing
1285 625 μM P (+P) or 5 μM P (-P). Images were taken 6 d after transfer. Scale bar = 1 cm.
1286 **(D)** Primary root length after transfer. Root phenotyping of indicated lines was
1287 conducted 6 d after transfer. Boxes show the first quartile, median and third quartile;

1288 the whiskers show minimum and maximum values; n = 20 plants. Different letters
1289 represent significant differences between treatments and lines according to two-way
1290 ANOVA followed by Tukey's HSD test at $P<0.05$. **(E)** Appearance of plants subjected
1291 to nickel (Ni) toxicity. After a pre-culture of 6 d, the seedlings of wild-type (Col-0),
1292 *pdx1.1-3*, *PDX1.1OE-L5*, *PDX1.1OE-L15* and *PDX1.1OE-L8* were transferred to half-
1293 strength MS medium in the absence (- Ni) or presence (+ Ni) of 75 μ M Ni. Images
1294 were taken 6 d after transfer. Scale bar = 1 cm. **(F)** Primary root length after transfer.
1295 Root phenotypes were recorded 6 d after transfer. Boxes show the first quartile,
1296 median and third quartile; the whiskers show minimum and maximum values; n = 20
1297 plants. Different letters represent significant differences between samples according
1298 to two-way ANOVA followed by Tukey's HSD test at $P<0.05$.

1299

1300 **Table S1. Chemical Information.**1301 **Table S2. Protocol for fixation, dehydration and embedding of root tissue.**1302 **Table S3. Primers used in this study.**1303 **Data Set S1. Information on ammonium-responsive genes used for the mutant**
1304 **screening in this study.**

1305

1306 REFERENCES

- 1307 Auh, C.K., and Murphy, T.M. (1995). Plasma-membrane redox enzyme is involved in
1308 the synthesis of O_2^- and H_2O_2 by phytophthora elicitor-stimulated rose cells.
1309 Plant Physiol 107:1241-1247.
- 1310 Bai, L., Ma, X., Zhang, G., Song, S., Zhou, Y., Gao, L., Miao, Y., and Song, C.P.
1311 (2014). A receptor-like kinase mediates ammonium homeostasis and is
1312 important for the polar growth of root hairs in Arabidopsis. Plant Cell 26:1497-
1313 1511.
- 1314 Balzergue, C., Dartevielle, T., Godon, C., Laugier, E., Meisrimler, C., Teulon, J.M.,
1315 Creff, A., Bissler, M., Bouchoud, C., Hagege, A., et al. (2017). Low phosphate
1316 activates STOP1-ALMT1 to rapidly inhibit root cell elongation. Nat Commun
1317 8:15300.
- 1318 Bhosale, R., Giri, J., Pandey, B.K., Giehl, R.F.H., Hartmann, A., Traini, R., Truskina,
1319 J., Leftley, N., Hanlon, M., Swarup, K., et al. (2018). A mechanistic framework
1320 for auxin dependent Arabidopsis root hair elongation to low external
1321 phosphate. Nat Commun 9:1409.
- 1322 Bielach, A., Podlesakova, K., Marhavy, P., Duclercq, J., Cuesta, C., Muller, B.,
1323 Grunewald, W., Tarkowski, P., and Benkova, E. (2012). Spatiotemporal
1324 regulation of lateral root organogenesis in Arabidopsis by cytokinin. Plant Cell
1325 24:3967-3981.
- 1326 Bilski, P., Li, M.Y., Ehrenshaft, M., Daub, M.E., and Chignell, C.F. (2000). Vitamin B6
1327 (pyridoxine) and its derivatives are efficient singlet oxygen quenchers and
1328 potential fungal antioxidants. Photochem Photobiol 71:129-134.
- 1329 Boycheva, S., Dominguez, A., Rolcik, J., Boller, T., and Fitzpatrick, T.B. (2015).
1330 Consequences of a deficit in vitamin B6 biosynthesis de novo for hormone
1331 homeostasis and root development in Arabidopsis. Plant Physiol 167:102-117.
- 1332 Britto, D.T., and Kronzucker, H.J. (2002). NH_4^+ toxicity in higher plants: a critical
1333 review. J Plant Physiol 159:567-584.
- 1334 Buettner, G.R., Doherty, T.P., and Patterson, L.K. (1983). The kinetics of the reaction
1335 of superoxide radical with Fe(III) complexes of EDTA, DETAPAC and HEDTA.
1336 Febs Lett 158:143-146.
- 1337 Chu, X., Wang, J.G., Li, M., Zhang, S., Gao, Y., Fan, M., Han, C., Xiang, F., Li, G.,
1338 Wang, Y., et al. (2021). HBI transcription factor-mediated ROS homeostasis
1339 regulates nitrate signal transduction. Plant Cell 33:3004-3021.
- 1340 Coletto, I., Bejarano, I., Marin-Pena, A.J., Medina, J., Rioja, C., Burow, M., and
1341 Marino, D. (2021). *Arabidopsis thaliana* transcription factors MYB28 and
1342 MYB29 shape ammonium stress responses by regulating Fe homeostasis.
1343 New Phytol 229:1021-1035.
- 1344 Colinas, M., Eisenhut, M., Tohge, T., Pesquera, M., Fernie, A.R., Weber, A.P.M., and
1345 Fitzpatrick, T.B. (2016). Balancing of B-6 vitamins is essential for plant
1346 development and metabolism in Arabidopsis. Plant Cell 28:439-453.
- 1347 Colon-Carmona, A., You, R., Haimovitch-Gal, T., and Doerner, P. (1999). Spatio-
1348 temporal analysis of mitotic activity with a labile cyclin-GUS fusion protein.
1349 Plant J 20:503-508.
- 1350 Cruz, C., Bio, A.F.M., Dominguez-Valdivia, M.D., Aparicio-Tejo, P.M., Lamsfus, C.,
1351 and Martins-Loucao, M.A. (2006). How does glutamine synthetase activity
1352 determine plant tolerance to ammonium? Planta 223:1068-1080.
- 1353 Danon, A., Miersch, O., Felix, G., Camp, R.G., and Apel, K. (2005). Concurrent
1354 activation of cell death-regulating signaling pathways by singlet oxygen in
1355 *Arabidopsis thaliana*. Plant J 41:68-80.

- 1356 Dell'Aglio, E., Boycheva, S., and Fitzpatrick, T.B. (2017). The Pseudoenzyme
1357 PDX1.2 Sustains Vitamin B-6 Biosynthesis as a Function of Heat Stress. *Plant*
1358 *Physiol* 174:2098-2112.
- 1359 Dello Ioio, R., Linhares, F.S., Scacchi, E., Casamitjana-Martinez, E., Heidstra, R.,
1360 Costantino, P., and Sabatini, S. (2007). Cytokinins determine Arabidopsis root-
1361 meristem size by controlling cell differentiation. *Current Biology* 17:678-682.
- 1362 Dello Ioio, R., Nakamura, K., Moubayidin, L., Perilli, S., Taniguchi, M., Morita, M.T.,
1363 Aoyama, T., Costantino, P., and Sabatini, S. (2008). A genetic framework for
1364 the control of cell division and differentiation in the root meristem. *Science*
1365 322:1380-1384.
- 1366 Dixon, S.J., and Stockwell, B.R. (2014). The role of iron and reactive oxygen species
1367 in cell death. *Nat Chem Biol* 10:9-17.
- 1368 Dong, Q., Bai, B., Almutairi, B.O., and Kudla, J. (2021). Emerging roles of the CBL-
1369 CIPK calcium signaling network as key regulatory hub in plant nutrition. *J Plant*
1370 *Physiol* 257:153335.
- 1371 Duan, F., Giehl, R.F.H., Geldner, N., Salt, D.E., and von Wirén, N. (2018). Root zone-
1372 specific localization of AMTs determines ammonium transport pathways and
1373 nitrogen allocation to shoots. *PLoS Biol* 16:e2006024.
- 1374 Ferreira, F.J., and Kieber, J.J. (2005). Cytokinin signaling. *Curr Opin Plant Biol* 8:518-
1375 525.
- 1376 Fitzpatrick, T.B. (2011). Vitamin B6 in plants: more than meets the eye. *Adv Bot Res*
1377 59:1-38.
- 1378 Fitzpatrick, T.B., Amrhein, N., Kappes, B., Macheroux, P., Tews, I., and Raschle, T.
1379 (2007). Two independent routes of de novo vitamin B6 biosynthesis: not that
1380 different after all. *Biochem J* 407:1-13.
- 1381 Gazzarrini, S., Lejay, L., Gojon, A., Ninnemann, O., Frommer, W.B., and von Wirén,
1382 N. (1999). Three functional transporters for constitutive, diurnally regulated,
1383 and starvation-induced uptake of ammonium into Arabidopsis roots. *Plant Cell*
1384 11:937-947.
- 1385 Gjetting, K.S.K., Ytting, C.K., Schulz, A., and Fuglsang, A.T. (2012). Live imaging of
1386 intra- and extracellular pH in plants using pHusion, a novel genetically
1387 encoded biosensor. *J Exp Bot* 63:3207-3218.
- 1388 Green, L.S., and Rogers, E.E. (2004). FRD3 controls iron localization in Arabidopsis.
1389 *Plant Physiol* 136:2523-2531.
- 1390 Guan, M., de Bang, T.C., Pedersen, C., and Schjoerring, J.K. (2016). Cytosolic
1391 glutamine synthetase Gln1;2 is the main isozyme contributing to GS1 activity
1392 and can be up-regulated to relieve ammonium toxicity. *Plant Physiol*
1393 171:1921-1933.
- 1394 Hachiya, T., Inaba, J., Wakazaki, M., Sato, M., Toyooka, K., Miyagi, A., Kawai-
1395 Yamada, M., Sugiura, D., Nakagawa, T., Kiba, T., et al. (2021). Excessive
1396 ammonium assimilation by plastidic glutamine synthetase causes ammonium
1397 toxicity in Arabidopsis thaliana. *Nat Commun* 12:4944.
- 1398 Hangarter, R.P., and Stasinopoulos, T.C. (1991). Effect of Fe-catalyzed
1399 photooxidation of EDTA on root-growth in plant culture media. *Plant Physiol*
1400 96:843-847.
- 1401 Havaux, M., Ksas, B., Szewczyk, A., Rumeau, D., Franck, F., Caffarri, S., and
1402 Triantaphylides, C. (2009). Vitamin B6 deficient plants display increased
1403 sensitivity to high light and photo-oxidative stress. *BMC Plant Biol* 9.
- 1404 Ishiyama, K., Inoue, E., Watanabe-Takahashi, A., Obara, M., Yamaya, T., and
1405 Takahashi, H. (2004). Kinetic properties and ammonium-dependent regulation

- 1406 of cytosolic isoenzymes of glutamine synthetase in Arabidopsis. *J Biol Chem*
1407 279:16598-16605.
- 1408 Jain, S.K., and Lim, G. (2001). Pyridoxine and pyridoxamine inhibits superoxide
1409 radicals and prevents lipid peroxidation, protein glycosylation, and (Na⁺+K⁺)-
1410 ATPase activity reduction in high glucose-treated human erythrocytes. *Free*
1411 *Radical Bio Med* 30:232-237.
- 1412 Jian, S.F., Liao, Q., Song, H.X., Liu, Q., Lepo, J.E., Guan, C.Y., Zhang, J.H., Ismail,
1413 A.M., and Zhang, Z.H. (2018). NRT1.1-related NH₄⁺ toxicity is associated with
1414 a disturbed balance between NH₄⁺ uptake and assimilation. *Plant Physiol*
1415 178:1473-1488.
- 1416 Jiang, C.F., Belfield, E.J., Mithani, A., Visscher, A., Ragoussis, J., Mott, R., Smith,
1417 J.A.C., and Harberd, N.P. (2012). ROS-mediated vascular homeostatic control
1418 of root-to-shoot soil Na delivery in Arabidopsis. *Embo J* 31:4359-4370.
- 1419 Ju, X.T., Xing, G.X., Chen, X.P., Zhang, S.L., Zhang, L.J., Liu, X.J., Cui, Z.L., Yin, B.,
1420 Christie, P., Zhu, Z.L., et al. (2009). Reducing environmental risk by improving
1421 N management in intensive Chinese agricultural systems. *P Natl Acad Sci*
1422 *USA* 106:3041-3046.
- 1423 Kannan, K., and Jain, S.K. (2004). Effect of vitamin B-6 on oxygen radicals,
1424 mitochondrial membrane potential, and lipid peroxidation in H₂O₂-treated U937
1425 monocytes. *Free Radical Bio Med* 36:423-428.
- 1426 Kehrer, J.P. (2000). The Haber-Weiss reaction and mechanisms of toxicity.
1427 *Toxicology* 149:43-50.
- 1428 Kempinski, C.F., Haffar, R., and Barth, C. (2011). Toward the mechanism of NH₄⁺
1429 sensitivity mediated by Arabidopsis GDP-mannose pyrophosphorylase. *Plant*
1430 *Cell Environ* 34:847-858.
- 1431 Khan, A.U., and Kasha, M. (1994). Singlet molecular-oxygen in the Haber-Weiss
1432 reaction. *P Natl Acad Sci USA* 91:12365-12367.
- 1433 Konishi, N., Ishiyama, K., Beier, M.P., Inoue, E., Kanno, K., Yamaya, T., Takahashi,
1434 H., and Kojima, S. (2017). Contributions of two cytosolic glutamine synthetase
1435 isozymes to ammonium assimilation in Arabidopsis roots. *J Exp Bot* 68:613-
1436 625.
- 1437 Koppenol, W.H., and Hider, R.H. (2019). Iron and redox cycling. Do's and don'ts.
1438 *Free radical biology & medicine* 133:3-10.
- 1439 Lager, I., Andreasson, O., Dunbar, T.L., Andreasson, E., Escobar, M.A., and
1440 Rasmusson, A.G. (2010). Changes in external pH rapidly alter plant gene
1441 expression and modulate auxin and elicitor responses. *Plant Cell Environ*
1442 33:1513-1528.
- 1443 Lee, Y., Rubio, M.C., Alassimone, J., and Geldner, N. (2013). A mechanism for
1444 localized lignin deposition in the endodermis. *Cell* 153:402-412.
- 1445 Leskovi, A., Zvari, K.M., Araya, T., and Giehl, R.F.H. (2020). Nickel toxicity targets
1446 cell wall-related processes and PIN2-mediated auxin transport to inhibit root
1447 elongation and gravitropic responses in Arabidopsis. *Plant Cell Physiol*
1448 61:519-535.
- 1449 Li, B.H., Li, G.J., Kronzucker, H.J., Baluska, F., and Shi, W.M. (2014). Ammonium
1450 stress in Arabidopsis: signaling, genetic loci, and physiological targets. *Trends*
1451 *in plant science* 19:107-114.
- 1452 Li, G., Zhang, L., Wang, M., Di, D., Kronzucker, H.J., and Shi, W. (2019). The
1453 Arabidopsis AMOT1/EIN3 gene plays an important role in the amelioration of
1454 ammonium toxicity. *J Exp Bot* 70:1375-1388.

- 1455 Li, Q., Li, B.H., Kronzucker, H.J., and Shi, W.M. (2010). Root growth inhibition by
1456 NH_4^+ in Arabidopsis is mediated by the root tip and is linked to NH_4^+ efflux and
1457 GMPase activity. *Plant Cell Environ* 33:1529-1542.
- 1458 Li, X. (2011). Histostaining for tissue expression pattern of promoter-driven GUS
1459 activity in Arabidopsis. *Bio-101* e93.
- 1460 Lima, J.E., Kojima, S., Takahashi, H., and von Wirén, N. (2010). Ammonium triggers
1461 lateral root branching in Arabidopsis in an AMMONIUM TRANSPORTER1;3-
1462 dependent manner. *Plant Cell* 22:3621-3633.
- 1463 Liu, Y., Lai, N., Gao, K., Chen, F., Yuan, L., and Mi, G. (2013). Ammonium inhibits
1464 primary root growth by reducing the length of meristem and elongation zone
1465 and decreasing elemental expansion rate in the root apex in Arabidopsis
1466 thaliana. *Plos One* 8:e61031.
- 1467 Liu, Y., and von Wiren, N. (2017). Ammonium as a signal for physiological and
1468 morphological responses in plants. *J Exp Bot* 68:2581-2592.
- 1469 Loque, D., Ludewig, U., Yuan, L., and von Wiren, N. (2005). Tonoplast intrinsic
1470 proteins AtTIP2;1 and AtTIP2;3 facilitate NH_3 transport into the vacuole. *Plant*
1471 *Physiol* 137:671-680.
- 1472 Lothier, J., Gaufichon, L., Sormani, R., Lemaitre, T., Azzopardi, M., Morin, H.,
1473 Chardon, F., Reisdorf-Cren, M., Avice, J.C., and Masclaux-Daubresse, C.
1474 (2011). The cytosolic glutamine synthetase GLN1;2 plays a role in the control
1475 of plant growth and ammonium homeostasis in Arabidopsis rosettes when
1476 nitrate supply is not limiting. *J Exp Bot* 62:1375-1390.
- 1477 Mahfouz, M.M., Zhou, S.Q., and Kummerow, F.A. (2009). Vitamin B6 compounds are
1478 capable of reducing the superoxide radical and lipid peroxide levels induced
1479 by H_2O_2 in vascular endothelial cells in culture. *Int J Vitam Nutr Res* 79:218-
1480 229.
- 1481 Meier, M., Liu, Y., Lay-Pruitt, K.S., Takahashi, H., and von Wirén, N. (2020). Auxin-
1482 mediated root branching is determined by the form of available nitrogen. *Nat*
1483 *Plants* 6:1136-1145.
- 1484 Moccand, C., Boycheva, S., Surriabre, P., Tambasco-Studart, M., Raschke, M.,
1485 Kaufmann, M., and Fitzpatrick, T.B. (2014). The pseudoenzyme PDX1.2
1486 boosts vitamin B-6 biosynthesis under heat and oxidative stress in Arabidopsis.
1487 *J Biol Chem* 289:8203-8216.
- 1488 Mooney, S., and Hellmann, H. (2010). Vitamin B6: Killing two birds with one stone?
1489 *Phytochemistry* 71:495-501.
- 1490 Mora-Macias, J., Ojeda-Rivera, J.O., Gutierrez-Alanis, D., Yong-Villalobos, L.,
1491 Oropeza-Aburto, A., Raya-Gonzalez, J., Jimenez-Dominguez, G., Chavez-
1492 Calvillo, G., Rellan-Alvarez, R., and Herrera-Estrella, L. (2017). Malate-
1493 dependent Fe accumulation is a critical checkpoint in the root developmental
1494 response to low phosphate. *P Natl Acad Sci USA* 114:E3563-E3572.
- 1495 Muller, J., Toev, T., Heisters, M., Teller, J., Moore, K.L., Hause, G., Dinesh, D.C.,
1496 Burstenbinder, K., and Abel, S. (2015). Iron-dependent callose deposition
1497 adjusts root meristem maintenance to phosphate availability. *Dev Cell* 33:216-
1498 230.
- 1499 Nakayama, S., Sugano, S.S., Hirokawa, H., Mori, I.C., Daimon, H., Kimura, S., and
1500 Fukao, Y. (2020). Manganese treatment alleviates zinc deficiency symptoms
1501 in Arabidopsis seedlings. *Plant Cell Physiol* 61:1711-1723.
- 1502 Nkebiwe, P.M., Weinmann, M., Bar-Tal, A., and Muller, T. (2016). Fertilizer
1503 placement to improve crop nutrient acquisition and yield: A review and meta-
1504 analysis. *Field Crop Res* 196:389-401.

- 1505 Patterson, K., Cakmak, T., Cooper, A., Lager, I., Rasmusson, A.G., and Escobar,
1506 M.A. (2010). Distinct signalling pathways and transcriptome response
1507 signatures differentiate ammonium- and nitrate-supplied plants. *Plant Cell*
1508 *Environ* 33:1486-1501.
- 1509 Percudani, R., and Peracchi, A. (2003). A genomic overview of pyridoxal-phosphate-
1510 dependent enzymes. *Embo Rep* 4:850-854.
- 1511 Qin, C., Qian, W.Q., Wang, W.F., Wu, Y., Yu, C.M., Jiang, X.H., Wang, D.W., and
1512 Wu, P. (2008). GDP-mannose pyrophosphorylase is a genetic determinant of
1513 ammonium sensitivity in *Arabidopsis thaliana*. *P Natl Acad Sci USA*
1514 105:18308-18313.
- 1515 Ragel, P., Rodenas, R., Garcia-Martin, E., Andres, Z., Villalta, I., Nieves-Cordones,
1516 M., Rivero, R.M., Martinez, V., Pardo, J.M., Quintero, F.J., et al. (2015). The
1517 CBL-interacting protein kinase CIPK23 regulates HAK5-mediated high-affinity
1518 K⁺ uptake in *Arabidopsis* roots. *Plant Physiol* 169:2863-2873.
- 1519 Raschke, M., Boycheva, S., Crevecoeur, M., Nunes-Nesi, A., Witt, S., Fernie, A.R.,
1520 Amrhein, N., and Fitzpatrick, T.B. (2011). Enhanced levels of vitamin B-6
1521 increase aerial organ size and positively affect stress tolerance in *Arabidopsis*.
1522 *Plant J* 66:414-432.
- 1523 Raschle, T., Arigoni, D., Brunisholz, R., Rechsteiner, H., Amrhein, N., and Fitzpatrick,
1524 T.B. (2007). Reaction mechanism of pyridoxal 5'-phosphate synthase -
1525 Detection of an enzyme-bound chromophoric intermediate. *J Biol Chem*
1526 282:6098-6105.
- 1527 Ristova, D., Carre, C., Pervent, M., Medici, A., Kim, G.J., Scalia, D., Ruffel, S.,
1528 Birnbaum, K.D., Lacombe, B., Busch, W., et al. (2016). Combinatorial
1529 interaction network of transcriptomic and phenotypic responses to nitrogen
1530 and hormones in the *Arabidopsis thaliana* root. *Science signaling* 9:rs13.
- 1531 Rogato, A., D'Apuzzo, E., Barbulova, A., Omrane, S., Parlati, A., Carfagna, S., Costa,
1532 A., Lo Schiavo, F., Esposito, S., and Chiurazzi, M. (2010). Characterization of
1533 a developmental root response caused by external ammonium supply in *Lotus*
1534 *japonicus*. *Plant Physiol* 154:784-795.
- 1535 Romheld, V., and Marschner, H. (1986). Evidence for a specific uptake system for
1536 iron phytosiderophores in roots of grasses. *Plant Physiol* 80:175-180.
- 1537 Roschztardt, H., Conejero, G., Curie, C., and Mari, S. (2009). Identification of the
1538 endodermal vacuole as the iron storage compartment in the *Arabidopsis*
1539 embryo. *Plant Physiol* 151:1329-1338.
- 1540 Sanchez-Barrena, M.J., Chaves-Sanjuan, A., Raddatz, N., Mendoza, I., Cortes, A.,
1541 Gago, F., Gonzalez-Rubio, J.M., Benavente, J.L., Quintero, F.J., Pardo, J.M.,
1542 et al. (2020). Recognition and activation of the plant AKT1 potassium channel
1543 by the kinase CIPK23. *Plant Physiol* 182:2143-2153.
- 1544 Shi, S.J., Xu, F.Z., Ge, Y.Q., Mao, J.J., An, L.L., Deng, S.J., Ullah, Z., Yuan, X.F., Liu,
1545 G.S., Liu, H.B., et al. (2020). NH₄⁺ toxicity, which is mainly determined by the
1546 high NH₄⁺/K⁺ ratio, is alleviated by CIPK23 in *Arabidopsis*. *Plants* 9.
- 1547 Smirnov, N., and Arnaud, D. (2018). Hydrogen peroxide metabolism and functions in
1548 plants. *New Phytol* 221:1197-1214.
- 1549 Stolz, J., and Vielreicher, M. (2003). Tpn1p, the plasma membrane vitamin B₆
1550 transporter of *Saccharomyces cerevisiae*. *J Biol Chem* 278:18990-18996.
- 1551 Straub, T., Ludewig, U., and Neuhaeuser, B. (2017). The kinase CIPK23 inhibits
1552 ammonium transport in *Arabidopsis thaliana*. *Plant Cell* 29:409-422.
- 1553 Sun, L., Di, D.W., Li, G.J., Kronzucker, H.J., Wu, X.Y., and Shi, W.M. (2020).
1554 Endogenous ABA alleviates rice ammonium toxicity by reducing ROS and free

- 1555 ammonium via regulation of the SAPK9-bZIP20 pathway. *J Exp Bot* 71:4562-
1556 4577.
- 1557 Sutton, M.A., Oenema, O., Erisman, J.W., Leip, A., van Grinsven, H., and Winiwarter,
1558 W. (2011). Too much of a good thing. *Nature* 472:159-161.
- 1559 Szydlowski, N., Burkle, L., Pourcel, L., Moulin, M., Stolz, J., and Fitzpatrick, T.B.
1560 (2013). Recycling of pyridoxine (vitamin B₆) by PUP1 in *Arabidopsis*. *Plant J*
1561 75:40-52.
- 1562 Tambasco-Studart, M., Titiz, O., Raschle, T., Forster, G., Amrhein, N., and Fitzpatrick,
1563 T.B. (2005). Vitamin B6 biosynthesis in higher plants. *P Natl Acad Sci USA*
1564 102:13687-13692.
- 1565 Thordal-Christensen, H., Zhang, Z.G., Wei, Y.D., and Collinge, D.B. (1997).
1566 Subcellular localization of H₂O₂ in plants. H₂O₂ accumulation in papillae and
1567 hypersensitive response during the barley-powdery mildew interaction. *Plant J*
1568 11:1187-1194.
- 1569 Tian, Q., Uhler, N.J., and Reed, J.W. (2002). *Arabidopsis* SHY2/IAA3 inhibits auxin-
1570 regulated gene expression. *Plant Cell* 14:301-319.
- 1571 Titiz, O., Tambasco-Studart, M., Warzych, E., Apel, K., Amrhein, N., Laloi, C., and
1572 Fitzpatrick, T.B. (2006). PDX1 is essential for vitamin B6 biosynthesis,
1573 development and stress tolerance in *Arabidopsis*. *Plant J* 48:933-946.
- 1574 Tsukagoshi, H. (2016). Control of root growth and development by reactive oxygen
1575 species. *Curr Opin Plant Biol* 29:57-63.
- 1576 Tsukagoshi, H., Busch, W., and Benfey, P.N. (2010). Transcriptional Regulation of
1577 ROS Controls Transition from Proliferation to Differentiation in the Root. *Cell*
1578 143:606-616.
- 1579 Vandesompele, J., De Preter, K., Pattyn, F., Poppe, B., Van Roy, N., De Paepe, A.,
1580 and Speleman, F. (2002). Accurate normalization of real-time quantitative RT-
1581 PCR data by geometric averaging of multiple internal control genes. *Genome*
1582 *Biol* 3.
- 1583 Wagner, S., Bernhardt, A., Leuendorf, J.E., Drewke, C., Lytovchenko, A., Mujahed,
1584 N., Gurgui, C., Frommer, W.B., Leistner, E., Fernie, A.R., et al. (2006).
1585 Analysis of the *Arabidopsis* *rsr4-1/pdx1-3* mutant reveals the critical function of
1586 the PDX1 protein family in metabolism, development, and vitamin B6
1587 biosynthesis. *Plant Cell* 18:1722-1735.
- 1588 Wasil, M., Halliwell, B., Grootveld, M., Moorhouse, C.P., Hutchison, D.C., and Baum,
1589 H. (1987). The specificity of thiourea, dimethylthiourea and dimethyl
1590 sulphoxide as scavengers of hydroxyl radicals. Their protection of alpha 1-
1591 antiproteinase against inactivation by hypochlorous acid. *Biochem J* 243:867-
1592 870.
- 1593 Watt, M., Silk, W.K., and Passioura, J.B. (2006). Rates of root and organism growth,
1594 soil conditions, and temporal and spatial development of the rhizosphere. *Ann*
1595 *Bot-London* 97:839-855.
- 1596 Xie, Y.J., Mao, Y., Xu, S., Zhou, H., Duan, X.L., Cui, W.T., Zhang, J., and Xu, G.H.
1597 (2015). Heme-heme oxygenase 1 system is involved in ammonium tolerance
1598 by regulating antioxidant defence in *Oryza sativa*. *Plant Cell Environ* 38:129-
1599 143.
- 1600 Xu, G.H., Fan, X.R., and Miller, A.J. (2012). Plant nitrogen assimilation and use
1601 efficiency. *Annual Review of Plant Biology* 63:153-182.
- 1602 Zheng, Z., Wang, Z., Wang, X.Y., and Liu, D. (2019). Blue light-triggered chemical
1603 reactions underlie phosphate deficiency-induced inhibition of root elongation of
1604 *Arabidopsis* seedlings grown in Petri dishes. *Mol Plant* 12:1515-1523.

1605 Zhu, C.Q., Zhang, J.H., Zhu, L.F., Abliz, B., Zhong, C., Bai, Z.G., Hu, W.J., Sajid, H.,
1606 James, A.B., Cao, X.C., et al. (2018). NH_4^+ facilitates iron reutilization in the
1607 cell walls of rice (*Oryza sativa*) roots under iron-deficiency conditions. *Environ*
1608 *Exp Bot* 151:21-31.
1609
1610

Journal Pre-proof

